A PRELIMINARY STUDY OF THE PHYSICAL PROPERTIES OF THE TERRA NOVA AND HIBERNIA OIL FIELDS IN THE JEANNE D'ARC BASIN, OFFSHORE NEWFOUNDLAND, CANADA

OPEN FILE
DOSSIER PUBLIC

2686

GEOLOGICAL SURVEY
COMMISSION GÉOLOGIQUE
OTTAWA

1993

HILMI S. SALEM
BEDFORD INSTITUTE OF OCEANOGRAPHY
GEOLOGICAL SURVEY OF CANADA
ATLANTIC GEOSCIENCE CENTRE
P.O. BOX 1006, DARTMOUTH, NOVA SCOTIA, B2Y 4A2, CANADA
TEL. (902) 426-7639, FAX. (902) 426-4465

CONTENTS

LIST OF TABLES

TABLE NO.

LIST OF FIGURES

FIGURE NO.

SYMBOLS

C = Electric conductivity (μS/cm) or $(\Omega.m)^{-1}$
CALI = Borehole diameter caliper log (mm)
CGLM = Conglomerate fraction (%)
CNL = Compensated neutron porosity log (%)
CSSL = Canadian Stratigraphic Service Ltd.
D = Grain diameter (μm) or (cm)
DEN = Density log (kg/m^3) or (gm/cm^3)
E = Young's modulus (Pa) or (Gpa) or ($dyne/cm^2$)
F = Formation resisitivity factor (dimensionless)
GR = Gamma ray log (API)
GSD = Mean grain size distribution (μm)
ILD = Deep induction resistivity lateral log (Ω.m)
ILM = Medium induction lateral log (Ω.m)
JDB = Jeanne d'Arc Basin
K, $\bar{K}$ = Permeability and average permeability in (mD) and/or (m^2)
K = Bulk modulus or incompressibility (Pa) or (GPa) or ($dyne/cm^2$)
K/μ = Bulk to shear modulus ratio (dimensionless)
KB = Kelly bushing (m)
LL8 = Lateral resistivity log 8 (Ω.m)
LLD = Deep lateral resistivity log (Ω.m)
LS = Limestone fraction (%)
MAD = Mean Absolute Deviation per point from the regression line
MARL = Marl fraction (%)
MLL = Microresistivity lateral log (Ω.m)
PC = Petro Canada
POR = Φ = Porosity (%)
SH = Shale fraction (%)
SILT = Silt fraction (%)
SON = Transit time sonic log (μs/m)
SP = Spontaneous potential log (mv)
S_p = Specific internal surface area of grains $(cm)^{-1}$
SS = Sandstone fraction (%)
S_w = Water saturation (%)
S_h = Oil or gas saturation (%)
T = Tortuosity (dimensionless)
T = Mean temperature of mud, mud filtrate and mud cake (°C)
V_p = Compressional wave velocity (m/s)
$(V_p)^2$ = Square of compressional wave velocity $(km/s)^2$
V_s = Shear wave velocity (m/s)
$(V_s)^2$ = Square of shear wave velocity $(km/s)^2$
V_p/V_s = Compressional to shear wave velocity ratio (dimensionless)
$\bar{VSH}$ = Volume of shale (content of shale and silt combined, %)
VSH = Average of volume of shale (content of shale and silt combined, %)
Z = Depth (m)

a,b = Coefficients in derived-empirical equations
a = Archie's coefficient (tortuosity factor)
a,b,c = Constants in Timur's-permeability equation
m = Archie's exponent (cementation factor)
n = Saturation exponent
Γ = Acoustic impedance $[(km/s)*(gm/cm^3)]$
x = Gamma log reading of clean sediments to gamma log reading of dirty sediments

λ = Lame's constant (Pa) or (GPa) or (dyne/cm^2)
μ = Shear modulus or rigidity (Pa) or (GPa) or (dyne/cm^2)
σ = Poisson's ratio (dimensionless)
β = Bulk compressibity (Pa)$^{-1}$ or (GPa)$^{-1}$ or (cm^2/dyne)
ρ = Bulk density (kg/m^3) or (gm/cm^3)
ρ_o = Bulk resistivity from ILD log (Ω.m)
ρ_m = Mud resistivity (Ω.m)
ρ_{mc} = Mud cake resistivity (Ω.m)
ρ_{mf} = Mud filtrate resistivity (Ω.m)
ρ_{sh} = Shale resistivity (Ω.m)
ρ_t = True formation resistivity (Ω.m)
ρ_w = Pore water resistivity (Ω.m)

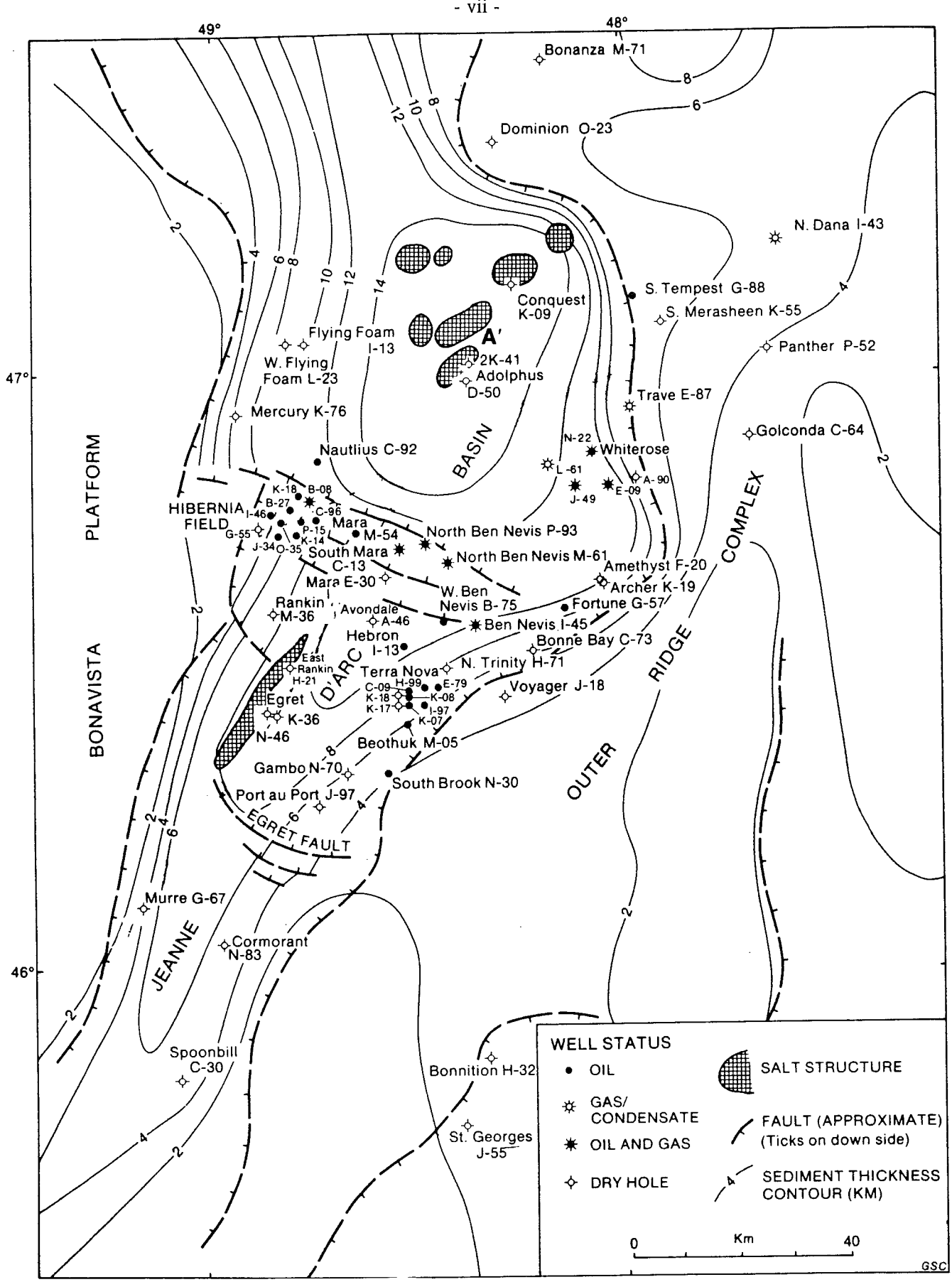

Location map of wells in the Jeanne d'Arc Basin (not indicated in the text, from McAlpine, 1990).

A PRELIMINARY STUDY OF THE PHYSICAL PROPERTIES OF THE TERRA NOVA AND HIBERNIA OIL FIELDS IN THE JEANNE D'ARC BASIN, OFFSHORE NEWFOUNDLAND, CANADA

HILMI S. SALEM
BEDFORD INSTITUTE OF OCEANOGRAPHY
GEOLOGICAL SURVEY OF CANADA
ATLANTIC GEOSCIENCE CENTRE
P.O. BOX 1006, DARTMOUTH, NOVA SCOTIA, B2Y 4A2, CANADA
TEL. (902) 426-7639, FAX. (902) 426-4465

ABSTRACT

Digital data from petrophysical logs of the Jeanne d'Arc Formation in the Terra Nova and Hibernia oil fields within the Jeanne d'Arc Basin (JDB) were analyzed. This work is a contribution to the JDB Hydrocarbon Charge Modelling Project. The purpose of this work is to achieve an assessment of physical properties of the Jeanne d'Arc reservoir and the saturating fluids.

Three groups of phyical parameters were deduced; petrophysical parameters, including porosity and permeability, and lithology variations; electric parameters, including water saturation, bulk and water resistivities, electric tortuosity, cementation factor, and specific internal surface area of grains and mean grain size; and elastic parameters, including the elastic moduli in terms of rigidity and compressibility, Poisson's ratio, Young's modulus, Lame's constant, and velocity ratio and acoustic impedance. Wide variations in the various physical parameters were obtained, which might be mainly attributed to the high heterogeneity of reservoir sediments.

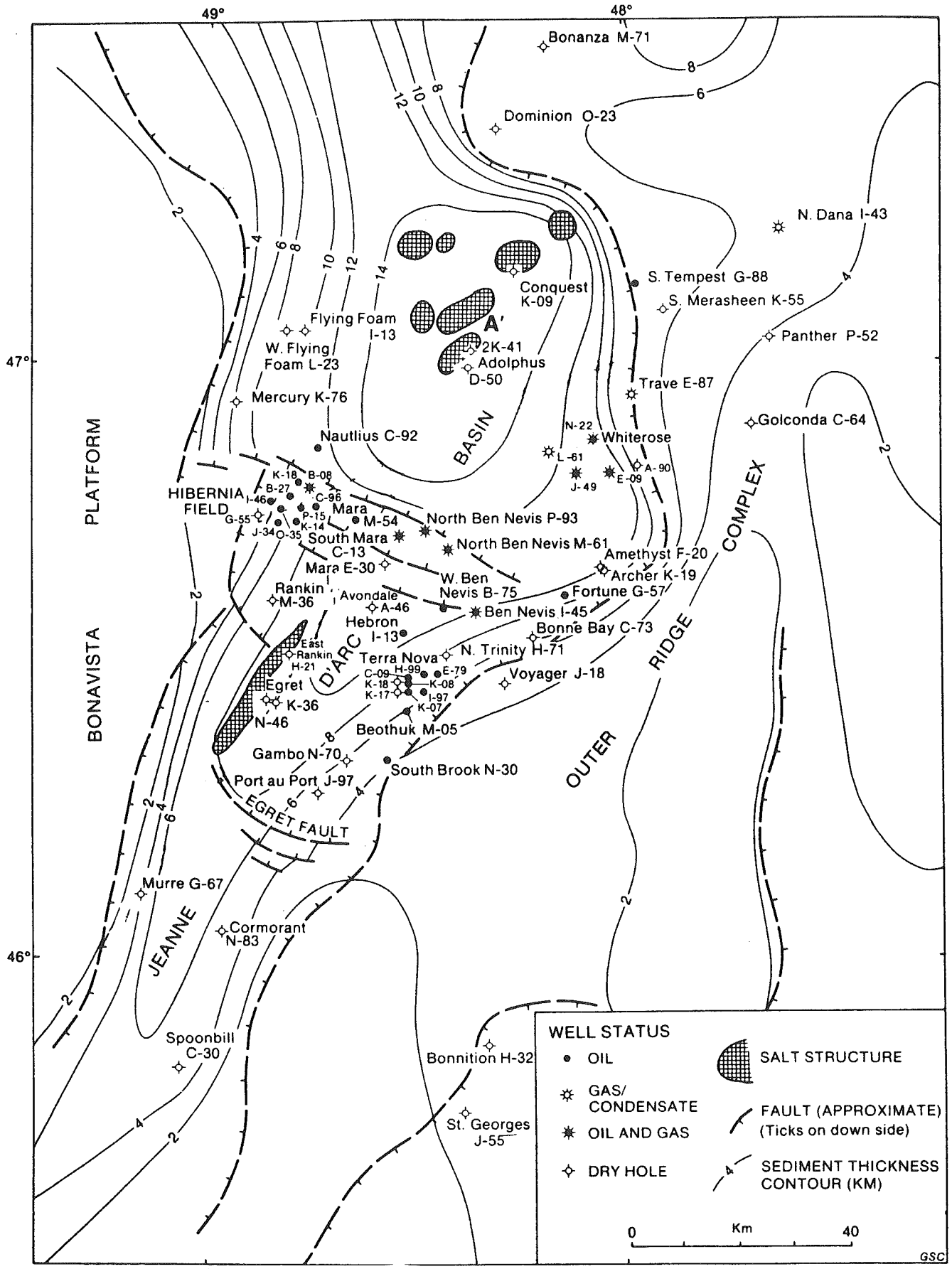

Location map of wells in the Jeanne d'Arc Basin (not indicated in the text, from McAlpine, 1990).

ABSTRACT

Digital data from petrophysical logs of the Jeanne d'Arc Formation in the Terra Nova and Hibernia oil fields within the Jeanne d'Arc Basin (JDB) were analyzed. This work is a contribution to the JDB Hydrocarbon Charge Modelling Project. The purpose of this work is to achieve an assessment of physical properties of the Jeanne d'Arc reservoir and the saturating fluids.

Three groups of phyical parameters were deduced; petrophysical parameters, including porosity and permeability, and lithology variations; electric parameters, including water saturation, bulk and water resistivities, electric tortuosity, cementation factor, and specific internal surface area of grains and mean grain size; and elastic parameters, including the elastic moduli in terms of rigidity and compressibility, Poisson's ratio, Young's modulus, Lame's constant, and velocity ratio and acoustic impedance. Wide variations in the various physical parameters were obtained, which might be mainly attributed to the high heterogeneity of reservoir sediments.

1. INTRODUCTION

Digital log data from the Jeanne d'Arc Formation in fourteen Hibernia and Terra Nova wells in the Jeane d'Arc Basin (JDB) were analyzed and interpreted. More details and interpretations will be given in several papers dealing comprehensively with specific physical parameters of the JDB. Analyses of the digital data were carried out using the Terra-Log program in addition to other programs developed to achieve the purpose of this study. In addition to the digital data, analog data, as well as lithological logs from cuttings analysis produced by the Canadian Stratigraphic Service Ltd. (CSSL) were used. This study concentrates on the Jeanne d'Arc reservoir interval of the Hibernia and Terra Nova oil fields in the JDB (Table 1.1). Table 1.2 shows the location information (latitude and longitude) for the various wells, in addition to some technical data (CSSL and Petro Canada PC) from drilling and logging processes. These data were used in the quantitative analysis of physical parameters.

2. METHODS

2.1 INPUT DATA AND GENERAL RELATIONSHIPS

The different logs used in calculation of physical properties are given in Tables 2.1 and 2.2, and the ranges and averages of measurements for the reservoir intervals of the Terra Nova and Hibernia wells are listed.

Generally the data given in Tables 2.1 and 2.2 show that the Jeanne d'Arc facies of both oil fields, Terra

Nova and Hibernia are characterized by wide variations in their physical properties. For example, the gamma ray values vary between about 8 and 135 API units, the bulk resistivity varies between about 0.1 and 9870 Ω.m, the bulk (matrix and fluid) density varies between about 1.35 and 3.72 gm/cm^3, the transit time of the compressional seismic wave varies between about 135 and 660 μs/m, or in terms of compressional wave velocity, as will be seen later, it varies between about 7350 and 1500 m/s, respectively. These wide variations of the measured physical properties are due to the lithological-mineralogical heterogeneity of the sediments, and due to the effect of the multi-saturating fluids (oil, gas and brine) filling the pore spaces. As will be seen later, these variations of the measured physical properties are reflected in the various calculated petrophysical, electric and elastic properties of the sediments.

To show the variations in some of the log measurements, Figure 2.1 is a plot of resistivity log (ILD) and spontaneous potential log (SP), density log (DEN) and sonic travel time log (SON), and sonic travel time log and neutron porosity log (CNL). The negative relationship between ILD and SP (Fig. 2.1-A) shows that by increasing the bulk resistivity (matrix and saturant resistivities), or by decreasing the bulk conductivity, the SP tends to decrease. This figure also shows that a range of SP between about -160 and -20 mv corresponds to a resistivity range between about 1 and 70 Ω.m. It can also be observed that 6 points of the 12 plotted points exhibit a range of SP between about -80 and -20 mv, corresponding to a resistivity range between about 1 and 10 Ω.m. Typical values of SP for shale and clean sand formations are between -15 and -100 mv, respectively (Desbrandes, 1985). The increase in electric conductivity and spontaneous potential is mainly attributed to the presence of conductive elements, either clay minerals or saline water or both, which helps the electric current to flow easily, leading to increase in the potential linked to the difference between the pore water and the mud filtrate. If the mud filtrate resistivity is higher than the pore water resistivity, the SP will be negative; if the mud filtrate resistivity equals pore water resistivity, the SP will be zero; if the mud filtrate resistivity is less than pore water resistivity, the SP will be positive. Therefore, the SP is negative if the pore water is saltier than the mud filtrate. Positive SPs are generally observed in the case of fresh water sands, or due to the presence of hydrocarbons in sandy formations. The presence of conductive elements such as clay minerals exisiting either in the form of shale layers, suspended particles in the fluid saturating the pores, or in the form of films coating the matrix particles, has an important influence on the relationship between spontaneous potential and electric conductivity.

Figure 2.1-B shows a decreasing relationship between bulk density (DEN) and sonic travel time (SON). This relationship shows a general range of DEN between about 2.25 and 2.65 gm/cm^3 corresponding to a general

range of SON between about 230 and 280 μs/m. The following values are the grain densities in gm/cm^3 for some composite minerals of sediments. Quartz = 2.65, calcite = 2.71, dolomite = 2.88, anhydrite = 2.98, halite = 2.04, and some clay minerals have grain densities between 2.12 and 2.79. Table 2.3 shows values of transit time (in μs/m), compressional wave velocity (in m/s) and bulk density (in gm/cm^3) for some selected dry and wet sediments and rocks, as well as fluids. Table 2.3 shows that the variation in travel time (seismic wave velocity) are affected by variations in bulk density due to variants in compaction and consolidation, saturation and type of saturant. One of the important factors which also affects the relationship between travel time or velocity of acoustic signal and density is the porosity level.

Figure 2.1-C shows a strong increasing relationship between sonic travel time (SON) and neutron porosity (CNL). This relationship corresponds to the decreasing relationship between seismic velocity (inverse of travel time) and porosity. Empirical equations linking the various logs plotted in Figure 2.1 were derived for the logs of spontaneous potential (SP) and deep resistivity (ILD), sonic travel time (SON) and bulk density (DEN), and neutron porosity (CNL) and sonic travel time (SON). These equations and their error coefficients (a and b), as well as the mean absolute deviations (MAD) of points from the regression lines are given in Table 2.4 (Eq. 2.1.1-2.1.3).

The average values of gamma ray (GR) logs show no systematic relationships with average values of other logs. For example, the relationships between GR and other logs such as SP, ILD, and CNL show increasing trends in the case of Terra Nova wells, and decreasing trends in the case of Hibernia wells. This is probably due to variations in amount and type of radioactive elements in the sediments of both oil fields.

2.2 OUTPUT DATA

By introducing the log measurements given in Table 2.1 into the Terra-Log program (1989), three groups of physical properties characterizing the sediments of Terra Nova and Hibernia were obtained for the reservoir intervals at 0.20 m increments. These properties are classified as petrophysical and lithological, electric, and elastic. This classification depends on the physical indications of the various properties in terms of petrophysical, electric and elastic responses of sediments in relation to their lithology and fluid saturants.

2.2.1 PETROPHYSICAL AND LITHOLOGICAL PROPERTIES

The petrophysical properties discussed in this part of the study are porosity in relation to the lithologic

variations investigated by the gamma ray (GR), sonic (SON), density (DEN), and compensated neutron porosity (CNL) logs. In addition, the shale content deduced from gamma ray logs, and the permeability calculated from porosity and water saturation are also discussed.

2.2.1.1 LITHOLOGY AND POROSITY

An estimation of the various lithological components in addition to porosity was achieved using the PETRA module in the Terra-Log program. Using the CSSL logs, digital and analog data, the lithological composition and porosity were obtained at different depths within different intervals of the various wells. This was achieved by introducing to the program the lithological components and porosity, for the various zones, in addition to their log readings to finally get a model of lithology and porosity being in agreement with the introduced data.

Two or more appropriate logs were chosen from the log measurements given in Table 2.1. It was found that the most effective logs in lithology and porosity calculations were the GR and SON logs. In case that SON logs were not available (Table 2.1), DEN and CNL logs were used. The lithological components used in the model representing the sediments in the different wells are: shale (SH), siltstone (SILT), sandstone (SS), marl (MARL), limestone (LS) and conglomerate (CGLM), as well as porosity (POR). It was found that the fewer components introduced, the better the results obtained. Therefore, the different zones were analyzed in small increments to reduce, as much as possible, the number of components, and consequently the errors in calculations.

To obtain a model of lithology and porosity satisfying the real situation, iteration processes were used. This type of analysis was done by solving a set of linear equations defining the lithology, porosity and their log readings. For example, 2.65SS + 2.71LS + 2.50SH + 1.00POR = DEN, where the constants in this equation are the density coefficients (in gm/cm^3) of each component, and DEN is the bulk density read from the density log. Each log used as input, either GR, SON or other, generates a similar equation with its own coefficients. Another equation used in the analysis implies that the sum of the components must be unity, i.e SS + LS + SH + POR = 1.0.

The success and accuracy of this analytical procedure is greatly dependent on choosing the appropriate coefficients, as well as on identifying the lithological components correctly. The accuracy of this procedure can also be adjusted by numerical diagnostic processes to assess the final solution reasonability. The diagnostics include the degree of agreement of the lithological-porosity model with the real situation of lithology and input measured data. Inconsistencies may result from bad log registrations, bad hole conditions, log miscalibrations, as well as poor

selection of the required coefficients. The diagnostic process is controlled by the sum deviation, which shows the deviation of analysis from the mathematically-ideal solution. The zero sum deviation indicates a very high degree of accuracy. The proportional variance as well as the error factor are other mathematical factors helping to improve the degree of accuracy. The proportional variance is an indicator of the degree of heterogeneity (or homogeneity) of the various lithological fractions included in the model to satisfy the real conditions. The error factor indicates the overestimation if this factor shifts from zero. Also the accuracy in analysis is highly dependent on the number of iterations used in computations.

A general summary of the results of this analysis including ranges of lithology fractions and porosity, as well as their averages are given in Table 2.5 and Table 2.6. The wide variation of lithology in the various wells and the presence, sometimes, of five lithological components or more, simply indicate the high degree of heterogeneity of the sediments, which is, in turn, reflected in the wide variations in porosity and, as will be seen later, in other physical properties. It is obvious from Table 2.5 that the shale and silt fractions are dominant, followed by the sandstone fraction. The silt fraction, as indicated by the CSSL, is generally shaly silt or silty shale. Comparing the Terra Nova and Hibernia oil fields, the Terra Nova has greater amounts of marl and conglomerate, and is generally characterized by higher amounts of shale.

Porosity in the Terra Nova and Hibernia fields varies between 0.0 and about 60% (Table 2.5), and ranges in average between about 7 and 18% (Table 2.6). This wide variation in porosity is attributed to the variations in grain size and lithology. The lowest values of porosity were obtained where considerable amounts of limestones and sandstones exist at greater depths. The highest values of porosity were generally obtained where high amounts of shale and silt exist at shallower depths. The traditionally accepted smooth porosity-depth decreasing curve may not represent the actual relationship at individual locations. The porosity sometimes decreases toward the inter-bedded permeable zones. A simple explanation for these porosity variations within the shales themselves or the sandstones might be attributed to variations in lithology or mineralogical composition or both. However, many instances showing no difference in composition or lithology with significant porosity differences can be attributed to the subsurface drainage and the pore pressures (Maghara, 1986). High values of porosity were also obtained even at very great depths. This is probably due to continuous deposition and burial causing the deeper sediments to be overpressured. Because of uplift and erosional effects, the surface temperature will decrease, and consequently the pore spaces may expand. In his study of overpressuring in the Venture gas field offshore Nova Scotia, Canada,

Mudford (1990) pointed out that the relatively rapid sedimentation rates in past geological times lead to the generation of overpressures.

Later in the permeability section, various relationships between porosity, permeability and the lithological fractions including shale, sandstone, silt and limestone are demonstrated and discussed.

The shale content (volume of shale, VSH) was calculated again according to the following equation (Terra-Log, 1989):

$$VSH = 0.33[2^{2X} - 1], \text{ where:} \qquad 2.2.1.1.1$$

x = Gamma log reading of clean sediments/Gamma log reading of dirty sediments.

Table 2.7 shows that the shale content calculated according to Equation 2.2.1.1.1 is generally greater than 90%. This high range of VSH might reflect the shales as total existing in the forms of suspended and structural shale, silty shale, shaly silt, sandy shale, shaly sand, limy shale, and shaly limestone.

2.2.1.2 PERMEABILITY

Permeability (K) is a very important parameter in petrophysics. It is one of the physical parameters which can't be easily deduced by log measurements. Most of the methods used to obtain permeability are based on empirical relationships. In addition to laboratory measurements, permeability can be obtained indirectly from the seismic attenuation method. However, because the laboratory meaurements of permeability were not used, the empirical equation given by Timur (1968) was used. This equation (2.2.1.2.1) generates an estimation of permeability (K) in mD based on porosity (Φ) in % and water saturation (S_w) in %. Timur's equation can be expressed as follows:

$$K = a(\Phi)^b/(S_w)^c, \text{ where: } a = 0.136, b = 4.40, \text{ and } c = 2.0 \qquad 2.2.1.2.1$$

It is worth indicating that derivation of (a, b, and c) coefficents from relationships between porosity and water saturation based on laboratory measurements is an important step to calibrate the present results of permeability. To obtain permeability (K), the calculated porosities given in Table 2.5, as well as the calculated water saturation values, disussed later, were introduced in Equation 2.2.1.2.1. The ranges and averages of permeability are summarized in Table 2.7. The calculated values of permeability generally range between 0.1 and about $1.52*10^4$ mD (between $9.87*10^{-17}$ and $1.50*10^{-10}$ m^2). Desbrandes (1985) pointed out that reservoir permeability, in general, varies between 0.1 and more than $1.0*10^4$ mD depending on reservoir lithology. The smallest value of permeability

obtained is 0.1 mD or $9.87*10^{-17}$ m^2. This value is the lowest limit that can be calculated by the Terra-Log program. However, Katsube et al. (1991) obtained extremely low values of permeability between $1.0*10^{-22}$ and $7.0*10^{-22}$ m^2 for cores taken from three wells on the Scotian Shelf at depths between 4500 and 5600 m. They attributed their extremely low permeabilies to the very tortuous paths connecting the pore spaces. They estimated an error value of up to 50%. However, Davis and De Wiest (1966) gave a permeability value of montmorillonite clay as low as $9.9*10^{-18}$ m^2 or 10^{-5} Darcy.

The wide range of permeability obtained is attributed to many reasons such as variations of pore geometry in terms of pore network, porosity, and tortuosity, specific surface area of grains and grain size. In addition, it is strongly influenced by lithology variations. As seen in Table 2.7, permeability in general is low or, in some cases, very low. This is due to the effects of overburden pressure and presence of shale in very high percentages.

Figure 2.2 shows various relationships between the averages of Φ and K (Table 2.6 and Table 2.7), and the averages of the various lithological fractions of sediments (Table 2.6). Emperical equations expressing the general trends of the regression lines of the various plots were derived. The equations are given in the same figures and summarized in Table 2.8. Regarding the various plots in Figure 2.2, the following features can be observed:

* Scattering is highly characteristic of the various relationships. This might be attributed to the fact that these relationships present the average values of the various quantities. In addition, the variations in surface area and size of composite grains of the different fractions of sediments is a main factor producing this high scattering.

* There is no general or consistent trend between porosity and permeability on the one hand, and lithology fractions on the other. It can be seen that porosity increases with increase of shale, sandstone, and silt fractions (Fig. 2.2-A, 2.2-C, and 2.2-E, respectively), whereas it shows no trend with the limestone content (Fig. 2.2-G). Regarding the permeability (K), it can be seen that K shows no trend at all. It slightly increases with increase of shale content (Fig. 2.2-B), and clearly decreases with increase of silt content (Fig. 2.2-F). As will be seen later, if shale and silt fractions were added together and considered as one fraction, from the point of view that they generally show the same readings of physical parameters, especially gamma ray and sonic transit time, it can be concluded that permeability decreases with increase of shale and silt contents. Permeability slightly decreases with increase of sandstone content (Fig. 2.2-D), and obviously increases with increase of limestone content (Fig. 2.2-H). This can be attributed to the fact that the sandstone is highly compressed due to the effect of overburden pressure, hence it shows a weak decreasing relationship with permeability. Increase of permeability with limestone content could be

attributed to the fact that, due to the effect of high overburden pressure and compressional stresses, new fractures might be created producing additional framework channels for fluid flow.

* The empirical equations, given in the same figures and summarized in Table 2.8 (Eq. 2.2.1.2.2-2.2.1.2.9), show that the plotted points of permeability in relation to lithological fractions exhibit high deviations (MAD) from the regression trend lines, and high errors in the a and b equation coefficients. The error values of a and b are generally higher than the coefficients themselves. Mathematically this indicates that the permeability relationships with lithological fractions are insignificant.

* In addition to the foregoing mentioned reasons, the high scattering in permeability relationships might also be attributed to the use of Timur's empirical equation in this study. The constants used in this equation are default ones, which probably do not strongly correspond to the sediments under study. In addition to the constants, Timur's equation takes into account the water saturation and porosity. The accumulated errors produced from porosity and water saturation calculations, in addition to the default constants, are other factors responsible to some extent for the high, scattered permeability-lithological fractions relationships.

* In conclusion, despite the high scattering in the relationships between porosity and permeability in respect to lithology, the porosity-lithology relationships show more reasonable results than permeability-lithology relationships. The imprecision in permeability relationships could be due to many factors such as drainage flow which is changed from layer to layer, and from zone to zone, and from well to well due to pressure variation. The characters of both dispersed and continuous phases will strongly affect the permeability relationships. These characters include, for example, compressibility of solid and fluid materials, viscosity and density of muli-phase fluids (brine, oil, and gas), pore geometry and fabric of sediments, temperature of saturants and containing-formations, and size and specific internal surface area of composite grains.

Figure 2.3 summarizes the relationships between porosity (Φ), permeablity (K) and shale content (VSH) for the Terra Nova and Hibernia oil fields. Figure 2.3-A shows the general relationship between Φ and K for all the lithological fractions together. A slightly decreasing relationship between Φ and K can be observed. This relationship can be expressed as follows:

$$\Phi = 1.427*10^{+1} - 2.661*10^{-3}\ K, \text{ where:} \qquad 2.2.1.2.10$$

Φ in %, and K in mD.

Figure 2.3-B shows the general relationship between Φ and VSH. The values of the shale content presented in this

figure, as well as in Figure 2.3-C, are the average values of the total shale deduced from the gamma ray measurements. This figure shows an increasing trend between Φ and VSH. The line of regression of this relationship shows the following empirical equation:

$$\Phi = 3.597*10^{-1} + 3.355*10^{-1}\ VSH, \text{ where:} \qquad 2.2.1.2.11$$

Φ and VSH are in %.

Despite the high scattering in the relationship between K and VSH, a slightly decreasing trend (Fig. 2.3-C) between these quantities was obtained. This relationship between permeability and shale content may reflect a reasonable result. This relationship can be expressed in the following empirical equation:

$$K = 4.835*10^{+2} - 6.847\ VSH, \text{ where:} \qquad 2.2.1.2.12$$

K in mD and VSH in %.

2.2.2 ELECTRIC PROPERTIES

Electric properties including pore water resistivity (ρ_w), water saturation (S_w), cementation factor (m), formation resistivity factor (F), and electric tortuosity (T) were calculated using the resistivity log measurements given in Table 2.1. In relation to these electric properties and the previously calculated porosity and permeability, the specific internal surface area (S_p) of composite grains and the mean grain size distribution (GSD) of sediments were also calculated. Note that S_p and GSD are not electric properties, but they are considered here because of their linkage to the electric properties. Tables 2.9 and 2.10 show ranges and averages of the deduced parameters corresponding to the Terra Nova and Hibernia oil fields.

2.2.2.1 PORE WATER RESISTIVITY

The pore water resistivity (ρ_w) was calculated according to the modified Archie's formula (Eq. 2.2.2.1.1). Values of the tortuosity factor (a) of 0.65 and the cementation factor (m) of 2.15 were used. These values of a and m generally correspond to shaly sandstones. In addition to a and m, a resistivity log (ρ_o) representing the formation bulk resistivity and porosity (Φ), which was previously calculated, were also used. The Archie's equation, in terms of pore water resistivity (ρ_w), can be written as follows:

$$\rho_w = \rho_o\ (\Phi^m)/a \qquad 2.2.2.1.1$$

The average values of water resistivity (Table 2.10) at reservoir temperature have a range between 0.05 and 1.32

Ω.m. In terms of conductivity (C), it ranges between 20 and 0.76 $(\Omega.m.)^{-1}$, or $2*10^5$ and $7.6*10^3$ μS/cm, respectively. It is evident that the pore water is highly conductive or of low resistance, indicating high salinity. The high salinity of pore water might be attributed to continuous chemical reactions between the pore water and the matrix composed of various minerals, by means of the water circulation. The high salinity (high conductivity) of pore water, and the conductive clay minerals, are effective factors in transmitting electric current.

2.2.2.2 WATER SATURATION

Water saturation, in addition to the shale content, is considered an important quantity in reservoir evaluation. Water saturation (S_w) is defined as the ratio of the volume of water in the pore spaces to the total volume of pores. The volume of pores is defined as the total volume or bulk volume of a sample multiplied by porosity of the sample. S_w was calculated as a fraction and expressed as a percent or a fraction. The hydrocarbon saturation (S_h) can be expressed as: $S_h = 1 - S_w$.

The modified equation given by Simandoux (1963) for shaly sediments was employed in this study to calculate the water saturation. The shale may be laminated, dispersed or structural. The three coexisting forms of shale were taken into consideration when Simandoux gave his modified model to calculate the water saturation. Simandoux's model can be expressed as follows:

$$S_w = [(a\rho_w/\Phi^m)\ (1 - VSH)/[\rho_t + \{\rho_o\ VSH\ (1 - VSH)/2\rho_{sh}\}^n]^{0.5} - [\rho_o\ VSH\ (1 - VSH)/2\rho_{sh}]] \qquad 2.2.2.2.1$$

where: S_w = Water saturation as a fraction

a = Archie's coefficient (tortuosity factor) = 0.65

m = Archie's exponent (cementation factor) = 2.15

n = Saturation exponent = 2.00

Φ = Porosity in fraction

VSH = Volume of shale in fraction

ρ_w = Pore water resistivity in Ω.m

ρ_t = True formation resistivity in Ω.m

ρ_o = Bulk measured resistivity in Ω.m

ρ_{sh} = Shale resistivity in Ω.m.

The above equation shows that the calculation of water saturation clarifies the contribution of shale to conductivity

of the medium. It also shows that water saturation is affected, in addition to shale content, by many factors linked to the electric conductivity, including degree of cementation and pore geometry.

As seen in Table 2.9, water saturation has a range between about 1 and 100%. The averages of water saturation (Table 2.10) range between about 40 and 83%. These results suggest that the water saturating the pores occupies a very low to medium to high proportion of these pores. The remaining parts might be occupied by oil or gas.

2.2.2.3 FORMATION RESISTIVITY FACTOR AND CEMENTATION FACTOR

The ratio between the bulk resistivity (ρ_o) and the pore water resistivity (ρ_w) was originally given by Sundberg (1932). This ratio was later defined by Archie (1942) as the formation resistivity factor (F). This parameter in relation to other parameters is affected by the behavior of porous media, and depends on the intricate geometry of the pore channels. The formation factor was calculated in this study (Table 2.9) according to Archie's formula ($F = \rho_o/\rho_w$). Its average (Table 2.10) varies between about 35 and 2170. The ranges given in Table 2.9 show that F exhibits very few readings of values less than 1.0. This indicates that, where very clean and pure clays exist, the pore water resistivity is higher than the bulk resistivity. The extremely high values of F indicate very high bulk resistivity (resistive dispered phase) and very low pore water resistivity (conductive continuous phase). In the present study, this situation was mostly encountered at greater depths where limestones, clean sandstones and even shales exist. The high formation factors of shales indicate that at greater depths shales become more resistive. However, according to modified Archie's equation ($F = a/\Phi^m$) (Winsauer et al., 1952), the formation factor (F) is inversely related to porosity (Φ), and directly related to tortousity factor (a) and cementation factor (m). Since the formation factor (F) is dependent on bulk as well as electrolyte resistivities, it can be concluded (Table 2.10) that formation factor increases (higher resistivity) with increase of mean grain size. Sarma and Rao (1962) experimentally, and Salem (1990) practically, achieved the same results.

The cementation factor (m) was originally defined by Archie (1942). As previously seen, it was included in many functions describing the behavior of porous media when an electric current passes through. In addition to consolidation and compaction effects, the cementation factor is also affected by the fabric of sediments, including the degree of packing, texture, orientation, grain size distribution, sorting and sphericity-angularity of grains. The results of m, given in Table 2.9, show wide variation, including low and high extremes. If these extremes reflect

the reality, it can be said that the low values might be related to weakly cemented sediments, and the high values might be correlated to well consolidated and cemented dense sediments. The extreme values may be due to mistakes in calculations. The averages of m between about 1.6 and 3.1 (Table 2.10) are in good agreement with the values given in the literature (between 1 and 3).

2.2.2.4 TORTUOSITY

Knowledge of the formation factor (F) and porosity (Φ) helps to numerically evaluate, in terms of tortuosity (T), the behaviour of electric and hydraulic flow in porous media. Salem (1990) mathematically derived T, in relation to bulk and pore water resistivities and porosity, as $T = (F^*\Phi)^{0.5}$. When an electric or hydraulic current flows in a porous medium, it will face higher resistivity if low porosity exists. In this case, the current will be forced to take a longer, more tortuous path which, consequently, leads to an increase in resistivity.

The values obtained for the formation factor and porosity were introduced in the simple equation defining the tortuosity (mentioned above). The results (ranges and averages) are given in Table 2.9 and Table 2.10. It can be seen that tortuosity has extremely high and low values. The extremely high values might be attributed to sediments exhibiting very high formation factors and very low porosities. This condition satisfies, more or less, the coarse-grained sediments, mainly the sandstones and probably some of the limestones. Carman (1956) pointed out that one of the factors affecting the tortuosity is the variation in particle shape. He experimentally indicated that spherical particles have relatively low values of tortuosity, whereas angular particles show relatively higher values of tortuosity. The high tortuosity values of angular particles may be attributed to the difficulty of obtaining random packing. The extremely low values of tortuosity represent sediments exhibiting very low formation factors and relatively high porosities. This condition generally corresponds to the very fine and fine-grained particles of shales, clayey and silty shales. The averages obtained in this study range between about 2 and 4 (Table 2.10). Katsube et al. (1991), in their study on the tight shales at depth greater than 4000 m, obtained apparent tortuosities between 2.3 and 11.9, and a true tortuosity of 3.3. They suggested that the high values of tortuosity indicate a very complex network of flow paths with pocket pores. Generally, increased resistance can be noted for rocks characterized by more tortuous passages (Helander and Campbell, 1966).

2.2.2.5 SPECIFIC INTERNAL SURFACE AREA AND MEAN GRAIN SIZE

In petrophysics, the specific internal surface area (S_p) has important physical influences in relation to various physical properties of porous media. It is of particular importance since it is related to grain size variation and shape of particles, porosity, permeability, tortuosity and other properties. It also has a specific meaning in defining fluid-solid relations. Also, it has a characteristic relation to the surface electric and electrolytic conductance of clays and fine colloidal clay particles. This parameter is defined as the ratio between the total internal surface area of particles and the bulk volume of the porous material (Wyllie and Spangler, 1952; Pfannkuch, 1969). More details about the mathematical derivation of this parameter, as well as the theoretical and practical physical meanings are given in Salem (1990). It can be numerically derived from the grain size distribution (GSD) or vice versa. In this study, it was derived in relation to the formation resistivity factor, porosity, and permeability according to the following equation given by Chilingar et al. (1963), which is originally based on the well known Kozeny-Carman equation (Carman, 1937):

$S_p = 4.46*10^{10}/[F^{2.2}*\Phi^{1.2}*K]^{1/2}$, where: 2.2.2.5.1

S_p = Specific surface area in cm^{-1}

F = Formation resistivity factor, dimensionless

Φ = Porosity in fraction

K = Permeability in mD.

The previously deduced values of F, Φ, and K were introduced in Equation 2.2.2.5.1. The results of S_p (Table 2.9) show a very wide range generally between 0.5 and about $1.6*10^5$ cm^{-1}. In his study of the glacial deposits in northern Germany, Salem (1990) obtained a range of S_p between 3 and $3*10^5$ cm^{-1} corresponding, respectively, to a range of grain size between 2 and $2*10^{-5}$ cm in diameter. These values correspond, respectively, to gravel and colloidal clay. The grain size in terms of diameter (D) was obtained in relation to the specific surface area according to the following equation given by Bear (1972):

$D = [(6 - 6\Phi)/S_p]$, where: 2.2.2.5.2

D = Diameter of grain in cm

Φ = Porosity in fraction

S_p = Specific surface area in cm^{-1}.

The derived grain size exhibits a range between 0.04 and 4940 μm in diameter. This range of grain size corresponds

to colloidal clay and coarse sand to fine gravel. The averages (Table 2.10) of mean grain size range between about 8 and 35 μm in diameter. This range corresponds to the grain size of clays, or to the equivalent, such as very fine calcite and dolomite. Katsube et al. (1991) experimentally obtained very small grain sizes agreeing with the present results. The deduced results of mean grain size suggest that the sediments are generally composed of clays, silts, fine to medium sands as well as calcites and dolomites. In conclusion, the clastic sediments under study are generally characterized by very high specific surface areas, and consequently by very fine to fine grained-particles. The degradaton of sediments towards the fine scale has a considerable effect on the various deduced petrophysical, electric and elastic properties.

2.2.2.6 RELATIONSHIPS BETWEEN ELECTRIC AND PETROPHYSICAL PROPERTIES (DEDUCED), AND PROPERTIES FROM LOG MEASUREMENTS

Relationships between various parameters (deduced and measured), including tortuosity (T), porosity (Φ), cementation factor (m), pore water resistivity (ρ_w), water saturation (S_w), formation resistivity factor (F), distribution of mean grain size (GSD), permeability (K), specific surface area (S_p), bulk resistivity (ILD), spontaneous potential (SP), gamma ray (GR), and bulk density (DEN), are plotted in Figures 2.4 and 2.5. These relationships are evaluated in terms of the mean absolute deviation (MAD) from the regression lines, and in terms of empirical equations showing the errors in the a and b coefficients in each equation (Table 2.11). The various plots show the following:

* Tortuosity (T) decreases with increase of porosity (Φ), cementation factor (m), and increase of water saturation (S_w) (Fig. 2.4-A, 2.4-B, 2.4-D, respectively). It slightly increases with increase of pore water resistivity (ρ_w) (Fig. 2.4-C). In the low range of Φ (Fig. 2.4-A) a gradual increase of T with decrease of Φ becomes well-marked. This result was also obtained by Carman's (1956) experimental work, and by Salem (1990) from field electric measurements. The T-Φ relationship also shows that the rate of increase in T accelerates rapidly when Φ becomes less than 10%, where low porosities are produced by increasing consolidation with depth. increase. Consolidated porous media attain greater tortuosities than unconsolidated porous media (Wyllie and Spangler, 1952). Hence, T progressively decreases as Φ increases indicating that the tortuous path of electric and hydraulic currents becomes longer and more complicated.

The decreasing relationship between tortuosity (T) and cementation factor (m) (Fig. 2.4-B) was also obtained by Wyllie and Rose (1950). According to their empirical formula, $m = [(\ln \Phi/T^{0.5})/\ln \Phi]$, tortuosity (T) increases

with decrease of the cementation factor (m). This type of relationship might be attributed to more conducting cement materials coating the grains, which in turn helps to conduct the electric current (lower tortuosity).

* The increasing relationship between tortuosity (T) and pore water resistivity (ρ_w) (Fig. 2.4-C) can be attributed to the fact that the increasing resistance (decreasing conductance) of pore fluid forces the electric current to pass through more tortuous and longer paths.

* Tortuosity of a continuous medium also shows some dependence on the variation of the degree of saturation (Perkins et al., 1956; Corey, 1977). As the degree of water saturation decreases (decrease of the wetting phase), fluid will take longer paths to flow, and the electric current will also follow in more tortuous paths (Fig. 2.4-D).

* The MAD as well as the error values of a and b coefficients in the derived empirical equations (Eq. 2.2.2.6.1-2.2.2.6.4) relating tortuosity and other parameters (Table 2.11) are reasonable.

* The formation resistivity factor (F) shows increasing relationships with bulk resistivity (ρ_o), distribution of mean grain size (GSD), and permeability (K) (Fig. 2.4-E, 2.4-F, 2.4-H, respectively). It also shows an inverse relationship with porosity (Φ) (Fig. 2.4-G). The direct relationship between F and ρ_o (Fig. 2.4-E) is due to the mathematical definition of the formation factor, i.e. [$F = \rho_o/\rho_w$]. The increase of formation factor with increase of grain size (GSD) (Fig. 2.4-F) can be explained in terms of surface electric conductance appearing on the surfaces of grains. In this case, the coarse-grained sediments exhibit low values of specific surface area and, in turn, they show low electric conductance or high resistance. Another explanation of the direct relationship between F and GSD is that porosity decreases by increasing the size of grains, hence they show higher formation factors than fine-grained sediments because the conduction is mostly via the water filling the pore spaces (Salem, 1990). Therefore, the conductivity primarily depends on the electrolyte within the pore spaces, especially if the pore water is highly saline as is the case in the present study. In fresh water formations, the electric conductivity is strongly dependent on the conductivity of clays, and on the electric charges held by the surfaces of clay particles. Generally, the total conductance (or resistance) appears to be equal to the sum of the conductance (or resistance) of both the solids and the saturating fluids (Patnode and Wyllie, 1950).

* The well-known inverse relationship (Archie, 1942) between the formation factor (F) and porosity (Φ), as obtained in Figure 2.4-G can be explained by the electric properties of most rocks and sediments, which mainly depend upon variations of electrolyte and bulk resistivities, and grain size.

* As previously pointed out, permeability (K) generally shows no consistent relationship with many other

parameters. The paradox in such relationships mainly depends on local petrophysical conditions, such as clay content, water salinity, grain size distribution and others. Various studies show direct correlations between K and F, and other studies show inverse correlations. More details about this controversy are given in Salem (1990). However, with dependence on a mathematical treatment between permeability, tortuosity, shape factor of grains, and formation factor given by Wyllie and Rose (1950), it can be suggested that the increase of permeability is related to decrease in tortuosity, and hence increase in formation factor (Fig. 2.4H) can be obtained. Archie (1942,1947) pointed out that the relationship between F and K is markedly dependent on the rock texture. This indicates that the variation in permeability with resistivity (in terms of the formation factor) is a function of the variations in both porosity and tortuosity.

* The MAD and the error values applying to the empirical equations between formation factor and other parameters (Eq. 2.2.2.6.5-2.2.2.6.8 in Table 2.11), seem to be generally high. These high values might be attributed to the fact that the sediments are highly shaly, which disturbs the relationships between formation factor, as a property of sediments resistance for electric current flow, and other parameters.

* The mean grain size distribution (GSD) shows considerable variations with different physical properties (Fig. 2.5A-H). Increasing trends are shown (Fig. 2.5-B, 2.5-C, 2.5-E, 2.5-F, 2.5-H) with permeability (K), tortuosity (T), spontaneous potential (SP), bulk resistivity (ILD) and bulk density (DEN), respectively. Also, decreasing trends are shown (Fig. 2.5-A, 2.5-D, 2.5-G) with porosity (Φ), specific surface area (S_p), and gamma ray (GR), respectively. The decrease of porosity by increasing the size of grains (Fig. 2.5-A) is accompanied by increase in tortuosity (Fig. 2.5-C). The increase of permeability with increase in grain size (Fig. 2.5-B) is attributed to the decrease of surface area of composite grains (Fig. 2.5-D). For example, clays (smaller grain size than sands) exhibit greater surface areas, and hence they exhibit less permeability than sands. These inter-relationships between grain size, porosity, permeability, tortuosity, and surface area of grains might be explained in terms of pore geometry (porosity), channel geometry (tortuosity), and the hydraulic conductance (linkage between porosity, permeability, tortuosity, and surface area of composite grains) of a medium composed of a network of channels connecting the pore spaces. Various studies were carried out (either experimentally, or theoretically, or in-situ measurements) and showed that permeability becomes progressively lower with decreasing grain size (Krumbein and Monk, 1942; Jones and Buford, 1951; Beard and Weyl, 1973; Paterson, 1983; Salem, 1990). Accordingly, one can expect that permeability decreases where the sediments become shaly, and it increases where the sediments become sandy. Increase of pressure (depth

increase), of course, is an important mechanism to decrease the permeability where packing and compaction tend to increase.

* Despite there being no known direct correlation between permeability, porosity (in relation to grain size), and the magnitude of spontaneous potential (SP), the polarity of the resultant potential depends on the nature of the solid (Serra, 1984). The slightly increasing relationship between SP and GSD (Fig. 2.5-E) is probably due to the fact that because of the ionization process, the surfaces of sandstone and limestone particles become negative, and clay surfaces become strongly negative as the light cations (Na^+, K^+, H^+, ...) tend to pass into solution. The SP is produced mainly by two main mechanisms; electrokinetic potential developed while the electrolytes penetrate the pores of the medium, and electrochemical potential developed when two fluids of different salinities are in direct contact or separated by a shaly membrane.

* The increasing relationship between resistivity (ILD) and GSD (Fig. 2.5-F) is due to the fact that the resistivity of a material generally increases by reduction of the amount of conductive elements, as in the case of fine-grained clays. The fine-grained particles are characterized by high specific surface areas on which more conductive ions are held and, in turn, electric current flows easier because of low resistance. The intercalation of sediments with different grain sizes, as well as the degree of coarseness of poorly-sorted sediments, in addition to variations in porosity and pore water resistivity, are all coexisting factors that could be responsible for resistivity variation in relation to grain size variation (Salem, 1990).

* The increasing relationship between bulk density (DEN) and GSD (Fig. 2.5-H) is attributed to the fact that the saturated coarse-grained sediments are mostly characterized by higher density than the saturated fine-grained sediments. Lennox and Carlson (1967) obtained higher densities for saturated sand than those of saturated silt and clay.

* The decreasing relationships (Fig. 2.5-A, 2.5-D, 2.5-G) of correlations between porosity (Φ), specific surface area (S_p), and gamma ray (GR), respectively, and GSD can be explained as follows: the decrease in grain size leads to more contact between the solid grains, consequently less packing and higher porosity are produced. In addition, the predominance of fine-grained platy sediments (shales) tends to increase the porosity. The smaller and flatter the particles, the greater the surface areas. Clay minerals, for example, due to their sheet structure, have an enormous specific surface areas compared to other materials. So far, the most important factor in evaluating the specific surface area in terms of grain size distribution is the clay content, where a decrease in grain size is produced.

Accordingly, an increase in gamma ray radiation is expected with the decrease of grain size (higher clay content).

* The MAD and errors in the a and b coefficients of the various equations (Eq. 2.2.2.6.9-2.2.2.6.16) given in Table 2.11, correlating grain size in terms of grain diameter (D) and other parameters, exhibit low, moderate and high values. This might be atrtributed to the complexity of relationships between the various physical properties of shaly sediments.

2.2.3 ELASTIC PROPERTIES

In the previous sections of this study, petrophysical and electric properties were deduced in relation to lithology and saturation. In this part of the study, elastic properties of the JDB sediments of the Terra Nova and Hibernia oil fields were deduced and interpreted in relation to lithology, saturation and other physical properties.

Elasticity is the property of resisting changes in size or shape and of returning to the undeformed condition when the external forces are removed. A perfectly elastic body is one which recovers completely after removal of a distorting stress. The relations between the applied forces and deformations are expressed in terms of stress and strain. The size and shape of a solid body can be changed by applying forces on the external surface of the body. These external forces are opposed by internal forces which resist the deformations. The body tends to return to its original condition when the external forces are removed. Liquids resist changes in size but not in shape. The propagation of a seismic wave through a body casuses the body to behave elastically. The stress-strain properties of a material which obeys Hook's law are specified by elastic moduli. The various elastic moduli, including Poisson's ratio, bulk modulus or its reciprocal (compressibility), shear modulus (rigidity), Young's modulus, and Lame's constant can be expressed in terms of each other, and derived in relation to compressional and shear wave velocities (V_p and V_s) (or transit times of both waves) along with bulk density (ρ). Seismic velocities and bulk densities provide sufficient information about the elastic behaviour of sediments in terms of elastic moduli.

2.2.3.1 POISSON'S RATIO

In principle, to obtain the elastic parameters, the transit time of both compressional and shear seismic waves are required in the case of log measurements, or seismic compressional and shear wave velocities in the case of "in-situ" field measurements or in the case of vertical seismic profiling. In the present study, because of the absence of shear wave measurements, it was attempted to indirectly estimate the various elastic parameters. This method

is not as good but it gives, to some extent, an acceptable estimation of the elastic parameters. By this method, Poisson's ratio (σ) was calculated using the previously calculated values of shale content (VSH). The following empirical formula representing a quantitative analysis for shaly sand and sandy shale formations, given by Crain (1986), was used:

$$\sigma = [VSH*0.125] + 0.27 \qquad 2.2.3.1.1$$

The above formula simply indicates that by increasing the shale content, the Poisson's ratio will increase, and the lowest derived value of σ is not smaller than 0.27. Therefore, σ exhibits a range between about 0.27 and 0.40 (Table, 2.12), and a range of averages between 0.31 and 0.33 (Table 2.13). Clark (1966) reported ranges of 0.18-0.28, and 0.23-0.31 corresponding, respectively, to sandstones and limestones. Poisson's ratio, as a measure of the change in shape, or a ratio of the lateral contraction or transverse strain to the longitudinal strain or extension resulting from a change in normal stress under compression or dilatation, has generally a wide range of variation between 0.0 and 0.5. The 0.5 value of σ indicates no volumetric change, as in the case of the fluids when they stressed. All the elastic properties, including σ, mostly depend on the lithological properties, degree of saturation, and type of saturant (gas, oil, water). However, any departure of the acoustic signal propagation from unsaturated to partially saturated, or to a totally saturated medium will increase the seismic wave velocity and, in turn, the Poisson's ratio tends to increase. Also, as indicated in the above equation, increasing the shale content tends to increase the Poisson's ratio. This is because shale can be simply deformed by the effect of stress applied. As will be seen later, the variation in Poisson's ratio can be explained in terms of the variations in other petrophysical and electric parameters.

2.2.3.2 COMPRESSIONAL WAVE VELOCITY

The compressional wave velocity (V_p) was directly deduced from the sonic transit time log (SON), as 10^5/SON. The velocity deduced ranges between 1515 and 7510 m/s (Table 2.12), with a range of averages between about 3650 and 4265 m/s (Table 2.13). These results indicate that sediments under study exhibit a wide range of velocities, from fluid velocity (see Table 2.3) to very high values corresponding to very consolidated sediments with extremely low porosity (zero or near zero). For purposes of comparison, some results of Gregory's and Pickett's (1977, 1963) experimental work, respectively, are presented in Table 2.14. The present results of V_p are shown to be higher than Gregory's results. This is due to the fact that Gregory's results do not represent sediments of high

densities and low porosities, similar to the present situation. The wide ranges of velocity reflected in the wide ranges of the elastic parameters deduced, can be attributed to variations in lithology and grain size, porosity, density, saturation and type of saturant. Compressional wave velocity shows a considerable change with change in compressibilities of both solid and fluid materials. Very low velocities might be due to gas saturating the pore spaces, or to the presence of very fine and soft clays. Very high readings of V_p might be attributed to very dense and hard rocks of extremely low porosities. High or very high velocity-materials might indicate hard, non-porous limestones and sandstones, or even shale under high overburden pressure. Gregory (1977) showed that fluid saturation effects on compressional wave velocity are much larger in low-porosity rocks than in high-porosity rocks (Table 2.14). In the general case, velocity increases with depth as porosity decreases. It is worth noting that in some results obtained in this study, V_p remains constant or shows a decrease at certain depths. This is probably due to the strong heterogeneity of the sediments, and to the type of saturant and degree of saturation. The dramatic decrease in V_p (increase in compressibility, as will be seen later) is associated with the change from water or oil saturation to gas saturation (Tatham, 1985).

2.2.3.3 VELOCITY RATIO AND SHEAR WAVE VELOCITY

The velocity ratio (V_p/V_s), compressional velocity (V_p) to shear velocity (V_s), was obtained according to the following formula:

$$V_p/V_s = [2(1-\sigma)/(1-2\sigma)]^{0.5} \qquad 2.2.3.3.1$$

The results show that this parameter generally ranges between 1.78 and 2.4 (Table 2.12). The results of V_p/V_s show that this parameter decreases with decrease of porosity as depth increases. The velocity ratio is a sensitive parameter to the degree of saturation as well as to the type of saturant. Since gas is more compressible than oil or water, the velocity ratio is lower for gas saturation than for oil or water saturation (Tatham, 1985). From log and laboratory measurements, Pickett (1963) observed that V_p/V_s can be used as a good indicator for lithology differentiation (Table 2.14). Gardner and Harris (1968) showed that velocity ratio values of less than 2.0 indicate either well consolidated rocks or gas saturation. Benzing (1978) further concluded that the presence of mud or shale in both carbonates and sandstones tends to increase the velocity ratio. By correlating the V_p/V_s results to the lithology logs of the various wells studied, it is found that the shaly zones exhibit V_p/V_s values higher than other zones of different sediments.

The shear wave velocity (V_s) was deduced from the velocity ratio by substitution of Equation 2.2.3.1.1 into

Equation 2.2.3.3.1. The results obtained for V_s (Tables 2.12 and 2.13) range between 775 and 4000 m/s, and range in average between about 1855 and 2220 m/s. Gregory (1977) obtained a range of V_s (Table 2.14) between 1097 and 2533 m/s, corresponding to sandstones saturated with different fluids.

2.2.3.4 SHEAR MODULUS OR RIGIDITY

Shear modulus (rigidity, μ) was calculated by introducing the bulk density (ρ in kg/m^3), taken from density log (DEN), and shear velocity (V_s in m/s), in the following equation:

$$\mu = (V_s)^2 * \rho \qquad 2.2.3.4.1$$

The values obtained for shear modulus and the other elastic moduli discussed below, are in $kg.m^{-1}.s^{-2}$, equal to one Pa. The shear modulus exhibits a range between about 1.6 and 41 GPa (Table 2.12), with a range of averages between about 8.2 and 13 GPa (Table 2.13). In $dyne/cm^2$, these results range between about $1.6*10^{10}$ and $41*10^{10}$. Gregory (1976) obtained μ values in a range of $3*10^{10}$ and $31*10^{10}$ $dyne/cm^2$ corresponding to high porosity-chalks, and low porosity-dense sandstones, respectively. The present results and Gregory's results indicate that rigidity increases by decreasing porosity. More information about shear modulus is given in Table 2.15. However, the shear strength and dynamic rigidity increase by increasing the effective pressure in terms of depth increase, as porosity is expected to decrease. The resistance to shear stresses is related to sliding and rolling friction between grains, and to the contact and inter-locking of solid particles (Salem, 1990). These factors depend on grain size and grain shape, in addition to the packing of grains. Decrease in shear modulus can be correlated to increase in porosity and to the presence of clays, as the interaction between pore fluid and clay producing softening of the matrix.

2.2.3.5 BULK MODULUS AND COMPRESSIBILITY

Bulk modulus (incompressibility, K) is a parameter describing the volume change due to compression and dilatation. It was calculated from bulk density (ρ), compressional wave velocity (V_p) and shear modulus (μ) according to the following equation:

$$K = \rho * (V_p)^2 * (4\mu/3) \qquad 2.2.3.5.1$$

In practice, this parameter is a function of porosity, grain size distribution, lithology, cementing material and effective pressure. The values obtained of bulk modulus (Table 2.12) range between about 4 and 99 GPa ($4*10^{10}$ and $99*10^{10}$ $dyne/cm^2$), with average values (Table 2.13) between about 20 and 30 GPa. The extremely high bulk modulus, shear

modulus - as previously seen, and Young's modulus and Lame's constant - as will be seen later, are attributed to the very low or zero-porosity of highly compacted sediments at great depths. Experimental results of ***K*** obtained by Gregory (1977) for various materials, including minerals and saturated sediments, as well as different types of fluids, are cited in Table 2.15.

The compressibility (β, reciprocal of bulk modulus, ***K***) defines the relationship between the pressure exerted on a body and the resulting change in its volume. From this study, it is found that β exhibits a range between about 0.01 and 0.259 GPa^{-1} ($1*10^{-12}$ and $2.59*10^{-11}$ Pa^{-1}), with a range of averages between about 0.035 and 0.054 GPa^{-1} ($3.5*10^{-12}$ and $5.4*10^{-12}$ Pa^{-1}). Examples of compressibility results obtained by Clark (1966) are cited in Table 2.15. The bulk compressibility of a saturated medium is a function of both matrix and fluid compressibilities. In the case of water saturating the pores, Shumway (1958) pointed out that the compressional wave velocity is highly affected by the high compressibility of water (between about $4.6*10^{-6}$ and $5.1*10^{-6}$ Pa^{-1}). It can be concluded that the type of saturant, the type of lithology and the magnitude of porosity are important factors that affect the bulk compressibility and, in turn, the velocity of compressional waves.

To correlate between bulk modulus (incompressibility, ***K***) and shear modulus (rigidity, μ), their ratio (K/μ) was calculated. It varies between 1.84 and 4.42 (Table 2.12), and ranges in average between 2.34 and 2.64 (Table 2.13). This ratio, besides the velocity ratio, is considered a good indicator for lithology, fluid saturation and porosity variations. Some relationships between this quantitiy and other parameters are demonstrated later.

2.2.3.6 YOUNG'S MODULUS AND LAME'S CONSTANT

Young's modulus (E) is defined as the ratio of normal stress to normal strain. It was calculated using the previously obtained results of Poisson's ratio (σ) and rigidity (μ) according to the following equation:

$$E = 2\mu(1+\sigma) \qquad 2.2.3.6.1$$

Table 2.12 shows that E exhibits a range between about 4 and 106 GPa, with a range of averages (Table 2.13) between about 22 and 34 GPa. These values reflect a wide range of variability of the stress applied and the strain developed due to presurization. Clark (1966) reported values of E (Table 2.15) between 19 and 100 GPa corresponding to different types of rocks. It is obvious that the deduced ranges in this study agree well with the values given by Clark. Clark's results indicate that sandstones exhibit the highest values of Young's modulus (E), followed by dolomites, limestones, dry shales, and finally wet shales. This indicates that the sandstones show high

resistance to the normal forces applied, and the wet shales show the lowest resistance, and in between the dolomites are followed by limestones, dry and wet shales. The decrease in Young's modulus and the increase in bulk compressibility might be caused by more fluid saturating the pore spaces (Mann and Fatt, 1960). The increase in Young's modulus can be attributed to reduction in the volume of pores due to increase in effective pressure by increase of depth. It can.be concluded that, since Young's modulus indicates the ratio of normal stress to normal strain, and since it includes the Poisson's ratio and the rigidity, or rigidity and incompressibility, in its mathematical definitions, the shales studied might be described as low resistance marerials. Variations in the physical and lithological properties of shales and other sedimets affect their elastic behavior and, in turn, the elastic parameters magnitudes will be changed.

Lame's constant (λ) was calculated in terms of incompressibility (K) and rigidity (μ) as follows:

$$\lambda = K - (2/3\mu) \qquad 2.2.3.6.2$$

Lame's constant (λ) varies between about 3 and 78 GPa (Table 2.12), with a range of averages (Table 2.13) between about 15 and 22 GPa. These results indicate that Lame's constant, as do other elastic parameters, increases with increase of effective pressure (depth), and with decrease of porosity.

2.2.3.7 ACOUSTIC IMPEDANCE

The acoustic impedance Γ, in (km/s)*(gm/cm^3), is not one of the elastic moduli. It is considered in this study as an elastic property, defined as the product of the compressional wave velocity (V_p) times the bulk density (ϱ). This parameter is related to the reflected energy and the incident energy in terms of the reflection coefficient. It exhibits a range between 3.2 and 19 (Table 2.12), and a range of averages (Table 2.13) between 8.3 and 10.7. This wide range of Γ reflects the wide range either in seismic velocity or in bulk density or in both. The high values indicate dense sediments of low porosity, and the low values indicate high porosity sediments, or sediments saturated with oil or gas.

2.2.3.8 RELATIONSHIPS BETWEEN VARIOUS ELASTIC, PETROPHYSICAL AND ELECTRIC PARAMETERS

Plots of double relationships are demonstrated in Figures 2.6 and 2.7 between the calculated petrophysical, electric and elastic parameters. The derived empirical equations (Eq. 2.2.3.8.1-2.2.3.8.12) correlating the various

parameters, as well as the mean absolute deviations (MAD), and error values in the a and b equation coefficients are given in Table (2.16). The various relationships and their derived equations suggest the following:

* The compressional wave velocity (V_p), is correlated with shale content (VSH) (Fig. 2.6-A, left) and with specific surface area of grains (S_p) (Fig. 2.6-A, right). Both parameters, VSH and S_p, show negative trends with V_p. The inverse relationship between V_p and VSH can be explained by the fact that the presence of clays reduces the seismic wave velocity because of their low bulk modulus (high compressibility) relative to other materials. The high compressibility of clays is attributed to their structure in comparison with sandstones and limestones. Different studies showed that the clay content tends to reduce the seismic velocity in both poorly and highly consolidated sediments (Minear, 1982; Castanga et al., 1985). The inverse relationship between V_p and S_p can be attributed, as previously discussed, to the fact that clay particles are characterized by extremely high specific surface areas. This result indicates that the seismic velocity increases by increase of grain size, as the surface area and the grain size are inversely related. The direct relationship between seismic velocity and grain size might be attributed to the higher stiffness of coarse-grained particles relative to fine-grained particles (Salem, 1990).

* A direct relationship between compressional wave velocity (V_p) and shear wave velocity (V_s) (Fig. 2.6-B, left), and an inverse one between V_p and porosity (Φ) (Fig. 2.6-B, right) are shown. The direct relationship between V_p and V_s is attributed to the fact that the sediments show increasing trends in incompressibility and rigidity (bulk modulus $\boldsymbol{K}$ and shear modulus μ) with increasing stress. The inverse relationship between V_p and Φ is directly related to increase in overburden pressure producing a decrease in pore spaces. From refraction measurements, Salem (1990) showed that the variations in V_p and V_s are dominantly correlated to variations in porosity.

* The third relationship shows an increasing trend between V_p and bulk modulus ($\boldsymbol{K}$) (Fig. 2.6-C, left), and a decreasing trend between V_p and water saturation (S_w) (Fig. 2.6-C, right). The increasing relationship between V_p and $\boldsymbol{K}$ is due to the direct derivation of K from V_p, density and shear modulus (Eq. 2.2.3.5.1). This trivial relationship is plotted here to show the variation in bulk modulus in relation to the compressional wave velocity for the different wells in the Terra Nova and Hibernia oil fields. The inverse relationship between V_p and S_w is due to the fact that by increasing the amount of saturation, the bulk modulus will decrease. As previously seen, the increase in shale content also decreases the V_p. The decrease in bulk modulus (decrease in velocity) indicates an increase in bulk compressibility (β) related to an increase in water saturation and shale content. This is because of the deformation produced by the propagation of seismic waves within saturated medium consisting of solid frame (matrix

particles) and fluid saturating the pore spaces. The type of fluid also has a significant role on bulk compressibility variation. In addition, the increase in water saturation softens the clay particles composing the shaly sediments. Consequently the bulk modulus will decrease and, in turn, the seismic velocity will also decrease. Han et al. (1986) pointed out that water saturation effects on seismic velocity in shaly sandstones are a function of different degrees of consolidation with respect to pore fluid and clay interactions.

* Relationships between porosity (Φ), compressibility (β), Poisson's ratio (σ), compressional to shear velocity ratio (V_p/V_s), bulk to shear moduli ratio (K/μ), square of compressional wave velocity $(V_p)^2$, square of shear wave velocity $(V_s)^2$, and acoustic impedance (Γ) are demonstrated in Figure 2.7. Direct relationships between Φ and β (Fig. 2.7-A, left), as well as between Φ and σ (Fig. 2.7-A, right) were obtained. The direct relationship between Φ and σ is due to the fact that higher pressure produces a reduction in porosity, as well as a reduction in compressibility. This means that more pressure is associated with higher seismic velocity, lower porosity, higher bulk and shear moduli (lower compressibility and higher rigidity). This indicates that any change in bulk compressibility is correlated to changes in fluid and solid compressibilities as well as to changes in porosity. The increase of compressibility with increase of porosity might be due to the deformation produced by the propagation of seismic waves. Hence a change in pore volume accompanying a change in bulk compressibility will be produced. From laboratory measurements on samples of limestones carried out by Koeffoed et al. (1963), and from refraction measurements carried out by Salem (1990), negative trends between porosity and Poisson's ratio were observed. Tatham (1985) pointed out that the softer the solids (finer grain size), the higher the porosity and the higher the Poisson's ratio, and the harder the solids (coarser grain size), the lower the porosity and the lower the Poisson's ratio. Davis and Schultheiss (1980) obtained very high Poisson's ratios corresponding to very highly porous clayey sediments. Gregory (1977) pointed out that Poisson's ratio tends to increase as porosity increases, but may increase, remain constant, or decrease as a function of pressure. This discussion suggests that no specific trend exists between porosity and Poisson's ratio, and this relationship (Φ-σ) mainly depends on the variations in pressure and clay content. Therefore, the increasing trend in the present study between Φ and σ is probably caused by variation in pressure, as well as by the presence of high amounts of clays in the sediments.

* Relationships in Figure 2.7-B (left and right) show, respectively, direct relationships between velocity ratio (V_p/V_s) and Poisson's ratio (σ), and between velocity ratio and bulk to shear modulus ratio (K/μ). Since the three parameters were directly derived from each other, such relationships show systematic and smoothly increasing trends.

Extension of the regression lines of both relationships to a Poisson's ratio value of 0.25 (Poisson's solid) will correspond to a V_p/V_s value of 1.732, as well as a K/μ value of 1.667. These figures indicate high inter-connection and great dependence of the three parameters.

* Figure 2.7-C (left and right) shows increasing relationships between the square of shear wave velocity $(V_s)^2$ and the square of compressional wave velocity $(V_p)^2$ on the left side, and between $(V_s)^2$ and acoustic impedance (Γ) on the right side. Krief et al. (1990) showed that cross plots of the squares of velocities contribute valuable information about lithology and fluid content, and the slopes of the regression lines have specific meanings. The present relationships show the following: A slope value of 3.30 represents the $(V_s)^2$-$(V_p)^2$ relationship, and a slope value of 1.59 represents the $(V_s)^2$-Γ relationship. The intercept value of the regression line with the square of the compressional velocity is about 11.6 $(km/s)^2$. The square root of this figure is about 3400 m/s (about 294 µs/m = 123 µs/ft). The intercept of the regression line with Γ (right Y axis) is about 7.8 (km/s)*(gm/cm^3), indicating a bulk density of about 2.3 gm/cm^3. These figures generally indicate shaly sediments saturated with gas. Note that these relationships are plotted for the average values of the three parameters (V_s^2, V_p^2, Γ) corresponding to 12 wells. If this technique is applied for a specific well with more data, more satisfying results can be obtained.

* The derived empirical equations and their corresponding mean absolute deviations (MAD), as well as the errors in the a and b coefficients are given in Table 2.16. Generally they indicate good relationships between the various parameters plotted. These results of the elastic properties, and the previous results of the petophysical and electric properties obtained, give a better understanding of the physical behavior of the Jeanne d'Arc Basin sediments and their saturating fluids.

3. THREE DIMENSIONAL REPRESENTATION

Some of the measured and deduced petrophysical, electric, and elastic properties of the Jeanne d'Arc Formation in the Terra Nova and Hiberina oil fields are presented in the form of three dimensional plots (Figs. 3.1 and 3.2). Fourteen relationships representing all the wells studied and relating the various parameters, lithology and depth, are plotted and discussed. Eight plots are given in Figure 3.1 representing the Terra Nova properties, including specific surface area (S_p in cm^{-1}), permeability (K in mD), distribution of mean grain size (GSD in µm), porosity (Φ in %), dimensionless tortuosity (T), bulk resistivity (ILD in Ω.m), water saturation (S_w in %), bulk density (ρ in kg/m^3), gamma ray (GR in API), shale content (SH in %), sand content (SS in %), spontaneous

potential (SP in mv), and water resistivity (ρ_w in Ω.m). Six plots given in Figure 3.2 representing the Hibernia properties, including dimensionless Poisson's ratio (σ), compressional wave velocity (V_p in m/s), bulk modulus (K in GPa), shear modulus (μ in GPa), acoustic impedance [Γ in (km/s)*(gm/cm^3)], Young's modulus (E in GPa), and the compressional wave velocity to shear wave velocity ratio (V_p/V_s). The various plots show the following:

3.1 TERRA NOVA FIELD

* Figure 3.1-A (C-09 well) shows seven peaks characterizing the permeability-surface area of composite grains-depth relationship. An increase in permeability is accompained by a decrease in surface area of composite grains. These peaks generally become very sharp at depths greater than 3460 m. Permeability varies from low to high at three different levels between about 3270 and 3360 m. The specific surface area tends to decrease (coarser grain size) with depth until it becomes nearly constant at a depth of about 3360 m. Below this depth it varies widely between low to high values.

* Figure 3.1-B (E-79 well) shows that porosity increases by decreasing the grain size of particles. Two sharp peaks and one wide peak at depths greater than 3280 m show medium to high porosity mostly corresponding to fine grained-sediments. The remaining part of the plot is generally characterized by smooth variations with smooth to moderate topography. At depth greater than 3200 m, porosity as well as grain size vary widely from very low to very high values.

* Figure 3.1-C (H-99 well) shows wide ranges of porosity and tortuosity. This model is characterized by many peaks at different depths. A characterized peak at a depth of about 3245 m can be seen on the left side of the plot corresponding to high porosity of about 30% and to a low tortuosity value of about 2.6. Generally, the plot shows an increase in tortuosity where porosity decreases by depth.

* Figure 3.1-D (I-97 well) shows a water saturation range between 1 and 100% with a bulk resistivity range between less than 1 and more than 2000 Ω.m. From right to left and from the top of the reservoir to the bottom, four narrow peaks and a very wide one appear in the plot indicating wide variation of resistivity in relation to wide variation in water saturation. The most characteristic wide peak, appearing at different depths, shows that water saturation starts from a moderate value of about 34% to complete saturation of 100%. This plot generally suggests that no specific trend exists between resistivity and water saturation in relation to depth variation.

* Figure 3.1-E (K-07 well) shows gamma ray increasing from about 28 to 100 API at different depths, where

density tends to be variable. This plot generally indicates no specific trend between density and gamma ray, and both quantities show considerable variation with depth.

* Figure 3.1-F (K-08 well) shows an increase in shale content (from zero to about 55%) correlating to a general decrease in sandstone content (from about 68 to 0.0%) in relation to depth decrease. This plot cleary indicates a systematic decrease of shale at the expense of a systematic increase of sandstone with depth.

* Figure 3.1-G (K-17 well) shows a plot relating permeability, porosity and shale content. It can be seen that porosity shows erratic variations between about 40 and 1.2% correlating to a permeability increase from 0.1 to 100 mD and to increase in shale content from 4.6 to about 25%. It can also be seen that by increasing the shale content, permeability tends to increase, while porosity tends to decrease systematically. This plot probably does not reflect the general character of the sediments under study, especially, as discussed earlier, that permeability decreases by increasing the shale content. For such relationship, the variations in depth, grain size, type of shales and their composition, and other lithological fractions, in addition to variations in other factors must be considered. Note that many permeability values are missed in this plot.

* Figure 3.1-H (K-18 well) shows the variation in spontaneous potential in relation to the water resistivity and depth variations. This plot shows a general increase of spontaneous potential (from about -164 to -135 mv correlating to an increase in depth and to an obvious decrease in pore water resistivity from about 8 to 0.01 Ω.m. The water resistivity shows three decreasing levels with respect to depth decrease.

3.2 HIBERNIA FIELD

* Figure 3.2-A (B-08 well) shows the relationship between Poisson's ratio, mean grain size and depth. This plot shows many peaks of low and high values of grain size at different depths, whereas Poisson's ratio does not correlate with grain size, but shows a decrease with depth increase. Since the Poisson's ratio was deduced in relation to shale content, its variations are related to shale content variation with depth. As previously discussed, Poisson's ratio for many reasons has no specific relationship with porosity, as a function of grain size variation.

* Figure 3.2-B (B-27 well) presents relationship between compressional wave velocity, porosity and depth. It can be seen that the seismic wave velocity increases from about 1500 to 7500 m/s at a small depth interval from 4163 to 4340 m. In addition, porosity varies between 50% to zero for the same depth interval. A characteristic peak of seismic velocity between about 3260 and 5260 m/s apears at different depths. An obvious increase in velocity

starts from about 5000 m/s to reach its maximum of more than 7500 m/s. Also, it can be seen that at this range of velocity (5000-7500 m/s) porosity exhibits a range of between 12 and 0.0%, corresponding to the total interval.

* Figure 3.2-C (C-96 well) shows the relationship between shear modulus, bulk modulus, and depth. This plot shows obvious increase in both moduli in relation to depth increase. It can also be seen that both parameters show their maximum values at greater depths, whereas the lowest values correlate to shallower depths. This plot simply indicates that rigidity (shear modulus) and incompressibility (bulk modulus) of sediments vary in the same manner in response to pressure variation.

* Figure 3.2-D (K-14 well) shows the relationship between shale content, acoustic impedance and depth. This plot shows that the shale content increases and decreases with depth, whereas the acoustic impedance (seismic velocity times density) generally increases with depth increase. The increase in acoustic impedance with depth is a direct function of increase in density or seismic velocity or both. This suggests that the increase in density and velocity with depth increase is a direct consequence of porosity decrease due to more compaction and cosolidation. It can also be seen that many positive peaks are spreading all over the plot, indicating different levels of variation in shale content and acoustic impedance in relation to depth increase.

* Figure 3.2-E (K-18 well) shows relationships between Young's modulus, mean grain size and depth. Generally, a decrease in grain size to about 130 μm is accompanied by a decrease in depth, then it gradually increases with increasing depth. Young's modulus shows two characteristic positive and negative peaks opposite to each other, with relatively the same range of values (between about 18 and 26 GPa). These peaks occur at deep and shallow depths.

* Figure 2.3-F (P-15 well) shows relationships between tortuosity, compressional to shear seismic velocity ratio in relation to depth. Tortuosity generally shows erratic variation with depth, while the velocity ratio shows a gradual increase with depth. Generally, this plot shows no clear relationship between tortuosity and velocity ratio.

It can be concluded that the three-dimensional plots, presented for the Terra Nova and Hibernia oil fields help to understand the inter-relationships between the different physical and lithological properties of sediments. They reflect conditions in the individual wells rather than the general behavior of the sediments of the Jeanne d'Arc Basin.

4. CONCLUSIONS

This study, as a contribution to the Hydrocarbon Charge Modelling Project of the Jeanne d'Arc Basin (JDB), offshore Newfoundland, was carried out to quantitatively analyze several petrophysical, electric and elastic properties in order to achieve better understanding of the physical behaviour of the Jeanne d'Arc Formation and its saturants. For this purpose, digital log data from 14 Terra Nova and Hibernia wells were analyzed and interpreted. The depth of the Jeanne d'Arc reservoir in the Terra Nova is between 2888 and 3556 m with a range of thickness between 290 and 389 m, while the depth in the Hiberia field is between between 3848 and 4763 m, with a range of thickness between 171 and 587 m.

Gamma ray, density, and sonic logs, compensated neutron porosity log and different types of electric logs were employed. Various petrophysical, electric and elastic parameters, in addition to the lithological composition, were deduced. The deduced parameters as well as the measured ones are presented in the form of tables including the ranges and averages corresponding to the various wells. Furthermore, the average values of the various parameters for all the wells studied were plotted in the form of cross plots. Empirical equations relating the plotted parameters, were derived. The empirical equations were evaluated in terms of the mean absolute deviation of the points from the regression lines, and in terms of the errors in the a and b coefficients of the empirical equations. Three dimensional plots were demonstrated for the physical properties for all the wells studied of the Terra Nova and Hibernia oil fields.

The Jeanne d'Arc Formation, under study, is composed of shales, sandstones, siltstones, and limestones. In some cases conglomerates and marls occur. The porosity, permeability, tortuosity, formation resistivity factor, cementation factor, water saturation, pore water resistivity, size of grains and their specific internal surface areas, compressional wave velocity, shear wave velocity and their ratio, Poisson's ratio, bulk modulus and its reciprocal compressibility, shear modulus (rigidity), bulk to shear modulus ratio, Young's modulus and Lame's constant were deduced.

Wide variations in all of the measured and deduced parameters were observed. This is because of the high degree of lithological heterogeneity characterizing the formation. The high shale content existing in both fields is one of the major factors responsible for high scattering in some of the relationships between different parameters. Also, the high shale content shows very considerable effects on the various parameters (measured and deduced).

In conclusion, the sediments consist of very fine to fine clays and fine to medium sands can generally be

described as low to medium porosity, low permeability, complicated tortuous networks and high specific surface areas. The inhomogeneity in sediment resistivity is a function of the pore water resistivity. The pore water is generally highly saline and highly conductive.

The Poisson's ratio and velocity ratio were deduced to indicate variations in lithology, grain size, and type of saturant. The various elastic parameters including the bulk modulus, shear modulus, Young's modulus and Lame's constant generally exhibit high values. This result is attributed to the high density, low porosity, and high seismic velocity of the sediments under high overburden pressure. However, laboratory measurements and calibration of the deduced parameters are recommended. More details about the physical properties and the physical behaviour of the Jeanne d'Arc Basin sediments and saturants are given in Salem (1992a, b, c, d, e, f) and Salem and Williamson (1992).

5. ACKNOWLEDGMENTS

The author expresses his appreciation and profound thanks to M.A. Williamson, K.D. McAlpine, K.C. Coflin, A.C. Grant, and J.A. Wade for their suggestions and discussions concerning this study, and for their reviewing the manuscript. Sincere thanks are also extended to A.E. Jackson and P.N. Moir for their help during the first few months in loading the digital data, and in solving technical hardware and software problems. Special thanks are also extended to Mrs. N. Koziel and Mrs. L. O'Neill. Thanks are also extended to all colleagues at the Atlantic Geoscience Centre of the Geological Survey of Canada at the Bedford Institute of Oceanography. This work is financed by the Natural Sciences and Engineering Research Council of Canada (NSERC), Ottawa.

6. REFERENCES

Archie, G.E., 1942, The electrical resistivity log as an aid in determining some reservoir chracteristics: Trans. of American Institute of Mining and Metallurgical Engineers, 146, 54-62.

Archie, G.E., 1947, Electrical resistivity an aid in core-analysis interpretation: Bull. of American Association of Petroleum Geologists, 31, 350-366.

Bear, J., 1972, Dynamics of Fluids in Porous Media: American Elsevier, N.Y., 764 p.

Beard, D.C., and Weyl, P.K., 1973, Influence of texture on porosity and permeability of unconsolidated sand: Bull. of American Association of Petroleum Geologists, 57, 349-369.

Benzing, W.M., 1978, V_p/V_s relationships in carbonates and sandstones - Laboratory data: Presented at the 48th Ann. Int. Mt. of the Society of Exploration Geophysicists, San Francisco, CA.

Bourbie, T., Coussy, O., and Zinszner, B., 1987, Acoustics of Porous Media: Editions Technip, Paris, 334 p.

Carman, P.C., 1937, Fluid flow through granular beds: Trans. of Institution of Chemical Engineers, 15, 150-156.

Carman, P.C., 1956, Flow of Gases Through Porous Media: Butterworths, London, 182 p.

Castagna, J.P., Batzle, M.L., and Eastwood, R.L., 1985, Relationship between compressional wave and shear-wave velocities in clastic silicate rocks: Geophysics, 50, 571-581.

Chilingar, G.V., Main, R., and Sinnokrot, A., 1963, Relationship between porosity, permeability, and surface areas of sediments: J. Sedimentary Petrology, 33, 759-765.

Clark, S.P., (ed.), 1966, Handbook of Physical Constants: Geological Society of America, Memior 97, 587 p.

Corey, A.T., 1977, Mechanics of Heterogeneous Fluids in Porous Media: Water Resources Publications, CO., 259 p.

Crain, E.R., 1986, The Log Analysis Handbook, Quantitative Log Analysis Methods, Vol.1: PennWell Pub. Comp., Tulsa, OK, 694 p.

Davis, A.M., and Schultheiss, P.J., 1980, Seismic signal processing in engineering site investigation - a case history: Ground Engineering, 13, 44-48.

Davis, S.N., and De Wiest, R.J.M., 1966, Hydrogeology: John Wiley & Sons, N.Y., 463 p.

Desbrandes, R., 1985, Encyclopedia of Well Logging: Inst. Franc. du Petrole Pub., Paris, 584 p.

Gardner, G.H.F., and Harris, M.H., 1968, Velocity and attenuation of elastic waves in sands: Trans. of Society of Professional Well Log Analysis, 9th Ann. Log. Symp., M1-19.

Gregory, A.R., 1976, Fluid saturation effects on dynamic elastic properties of sedimentary rocks: Geophysics, 41, 895-921.

Gregory, A.R., 1977, Aspects of rock physics from laboratory and log data that are important to seismic interpretation, 15-46: In Seismic Stratigraphy - Applications to Hydrocarbon exploration, Memior 26, edited by C.E. Pyton, Bull. of American Association of Petroleum Geologists, Tulsa, OK, 15-46.

Han, D.-H., Nur, A., and Morgan, D., 1986, Effect of porosity and clay content on wave velocities in sandstones: Geophysics, 51, 2093-2107.

Helander, D.P., and Campbell, J.M., 1966, The effect of pore configuration, pressure and temperature on rock

resistivity: Trans. of Society of Professional Well Log Analysis, W1-29.

Jones, P.H., and Buford, T.B., 1951, Electric logging applied to groundwater exploration: Geophysics, 16, 115-139.

Katsube, T.J., Mudford, B.S., and Best, M.E., 1991, Petrophysical characteristics of shales from the Scotian shelf: Sub. to Geophysics, 31 p.

Koeffoed, O., Oosterveld, M.M., and Alons, I.J.G., 1963, A laboratory investigation into the elastic properties of limestones: Geophysical Prospecting, 11, 300-312.

Krief, M., Garat, J., Stellingwerff, J., and Ventre, J., 1990, A petrophysical interpretation using the velocities of P and S waves (Full-Waveform Sonic): The Log Analyst, November-December, 355-369.

Krumbein, W.C., and Monk, G.D., 1942, Permeability as a function of the size parameters of unconsolidated sand: Trans. of American Institute of Mining and Metallurgical Engineers, 151, 153-163.

Lennox, D.H., and Carlson, V., 1967, Geophysical exploration for burried valleys in an area north of Two Hills, Alberta: Geophysics, 32, 331-362.

Maghara, K., 1986, Compaction and Fluid Migration, Practical Petroleum Geology: Developments in Petroleum Science, 9, Elsevier, Amsterdam, 319 p.

Mann R.L., and Fatt, I., 1960, Effect of pore fluids on the elastic properties of sandstone: Geophysics, 25, 433-444.

McAlpine, K.D., 1989, Lithostratigraphy of fifty-nine wells - Jeanne d'Arc Basin: Open File, Dossier Public, 2201, Geological Survey of Canada, Ottawa, 97 p.

McAlpine, K.D., 1990, Mesozoic stratigraphy, sedimentary evolution, and petroleum potential of the Jeanne d'Arc Basin, Grand Banks of Newfoundland: Geological Survey of Canada, Paper 89-17, 50 p.

Minear, M.J., 1982, Clay models and acoustic velocities: Pres. at the 57th Ann. Mt., Trans. of American Institue of Mining and Metallurgical Engineers, New Orleans.

Mudford, B.S., 1990, A one-dimensional, two phase model of overpressure generation in the Venture gas field, offshore Nova Scotia, Bull. of Canadian Petroleum Geology, 38, 246-258.

Paterson, M.S., 1983, The equivalent channel model for permeability and resistivity in fluid-saturated rocks - A preappraisal: Mechanical Materials, 2, 345-352.

Patnode, H.W., and Wyllie, M.R.J., 1950, The presence of conductive solids in reservoir rocks as a factor in electric log interpretation: Trans. of American Institute of Mining and Metallurgicalõ Engineers, 189, 47-52.

Perkins, F.M., Osoba, J.S., and Ribe, K.H., 1956, Risistivity of sandstones as related to the geometry of their

interstitial water: Geophysics, 21, 1071-1086.

Pfannkuch, H.-O., 1969, On the correlation of electrical conductivity properties of porous systems with viscous flow transport coefficients: Pres. at the 1st Int. Symp. on the Foundation of Transport Phenomena in Porous Media, International Association of Hydrological Research, Heifa, 42-54.

Pickett, G.R., 1963, Acoustic character logs and their application in formation evaluation: Trans. of American Institute of Mining and Metallurgical Engineers, 15, 659-667.

Salem, H.S., 1990, A Theoretical and Practical Study of Petrophysical, Electric, and Elastic Parameters of Sediments: Ph.D Thesis, Kiel University, F.R. Germany, Publ. by University Microfilms International (UMI), MI, USA, 200 p.

Salem, H.S., 1992a, Specific internal surface area and mean grain size of sediments in the Jeanne d'Arc Basin, offshore Newfoundland, Grand Banks, Canada: Submitted to The Log Analyst, 33 p.

Salem, H.S., 1992b, Physical, mathematical, and lithological aspects of electric and hydraulic tortuosities in the Jeanne d'Arc Basin, Offshore Newfoundland, Grand Banks, Canada: Submitted to The Log Analyst, 33 p.

Salem, H.S., 1992c, Derivation of the cementation factor (Archie's Exponent) and the Kozeny-Carman constant from well log data, and their dependence on lithology and other physical parameters: Submitted to the Journal of Petroleum Technology, 22 p.

Salem, H.S., 1992d, The electric and hydraulic anisotropic behaviors of the Jeanne d'Arc Basin sediments: Will be submitted to Geophysics, 30 p.

Salem, H.S., 1992e, Heterogeneity in lithology and physical properties of the Jeanne d'Arc Basin sediments: An approach from log data analysis: In preparation.

Salem, H.S., 1992f, Detailed results of petrophysical, electric and elastic properties for 14 Hibernia and Terra Nova wells in the Jeanne d'Arc Basin: In preparation.

Salem, H.S. and Williamson, M.A., 1992, Petrophysical, electric and elastic properties of Jeanne d'Arc Basin Reservoirs: Posters presented at the Oil and Gas Forum, February/92 in Calgary, and at the GAC-MAC Ann. Mt., May/92 in Wolfville, and at the Ann. Mt. of the AAPG, June/92 in Calgary and at the AGC Program Review in Dartmouth, Nova Scotia, November/92.

Sarma, V.V.J., and Rao, B., 1962, Variation of electrical resistivity of river sands, calcite and quartz powders with water content: Geophysics, 26, 470-479.

Schoen, J., 1983, Petrophysik: Akademie-Verlag, Berlin, 405 p.

Serra, O., 1984, Fundamentals of Well-Log Interpretation, 1. The Acquisition of Logging Data: Develp. in Petroleum Science. 15A, Elsevier, Amsterdam, 423 p.

Shumway, G., 1958, Sound velocity vs. temperature in water-saturated sidements: Geophysics, 23, 496-505.

Simandoux, P., 1963, Mesures dielectriques in milieu poreux, Application a mesure des saturations en eau, Etude du comportement des massifs argileux: Revue de I'institut Francais du Petrole, Suppl. Issue, 18, 193-215.

Sundberg, K., 1932, Effect of impregnating waters on electrical conductivity of soils and rocks: Trans. of American Institute of Mining and Metallurgical Engineers, 97, 367-391.

Tatham, R.H., 1985, Shear waves and lithology: In Seismic Shear Waves, Handbook of Geophysical Exploration, Part B, Applications, edited by K. Helbig and S. Treiter, 15B, Geophysical Press, London-Amsterdam, 87-133.

TerraLog/T.Log, 1989, The Advanced Well Log Analysis Program: In Terra Station, Terra Sciences, Denver, CO., 5-1 - 5-171.

Timur, A., 1968, An investigation of permeability, porosity and residual water saturation relationships: Trans. of Society of Professional Well Log Analyst, Ann. Log Symposium, June, J1-18.

Winsauer, W.O., Shearin, H.M., Masson, P.H., and Williams, M., 1952, Resistivity of brine-saturated sands in relation to pore geometry: Bull. of American Association of Petroleum Geology, 36, 253-277.

Wyllie, M.R.J., and Rose, W.D., 1950, Some theoretical considerations related to the quantitative evaluation of the physical characteristics of reservoir rocks from electrical log data: Trans. of American Institute of Mining and Metallurgical Engineers, 189, 105-118.

Wyllie, M.R.J., and Spangler, M.B., 1952, Application of electrical resistivity measurements to problem of fluid flow in porous media: Bull. of American Association of Petroleum Geologists, 36, 359-403.

Table (1.1): Depth and thickness of Jeanne d'Arc reservoir intervals of JDB wells (after McAlpine, 1989).

TERRA NOVA WELLS

No.	Name and Symbol	Total Depth (m)	Interval Studied (m)	Interval Thickness (m)
1.	Terra Nova C-09	3640	3188 - 3556	368
2.	Terra Nova E-79	3606	3125 - 3495	370
3.	Terra Nova H-99	3510	3072 - 3461	389
4.	Terra Nova I-97	3465	3080 - 3385	305
5.	Terra Nova K-07	3550	3114 - 3422	308
6.	Terra Nova K-08	4500	3188 - 3548	360
7.	Terra Nova K-17	3250	2888 - 3178	290
8.	Terra Nova K-18	3925	3050 - 3413	363

HIBERNIA WELLS

No.	Name and Symbol	Total Depth (m)	Interval Studied (m)	Interval Thickness (m)
1.	Hibernia B-08	4435	3848 - 4435	587
2.	Hibernia B-27	4380	4160 - 4380	220
3.	Hibernia C-96	4423	4193 - 4420	227
4.	Hibernia K-14	4079	3520 - 4056	536
5.	Hibernia K-18	5050	4055 - 4547	492
6.	Hibernia P-15	4410	4114 - 4258	171

Table (1.2): Well locations and some technical data used in log analysis (after Canadian Stratigraphic Service Ltd., CSSL, and Petro Canada, PC).

TERRA NOVA WELLS

No.	Name and Symbol	Latitude	Longitude	KB (m)	[ρ_m (Ω.m)	ρ_{mf} (Ω.m)	ρ_{mc}] at (Ω.m)	T (°C)
1.	Terra Nova C-09	N 46 28 10	W 48 30 59	24.5	0.12	0.10	0.26	13
2.	Terra Nova E-79	N 46 28 29	W 48 26 48	24.2	0.13	0.11	0.28	15
3.	Terra Nova H-99	N 46 28 29	W 48 28 50	24.0	0.11	0.10	0.20	18
4.	Terra Nova I-97	N 46 26 43	W 48 28 49	23.7	0.12	0.09	0.39	18
5.	Terra Nova K-07	N 46 26 44	W 48 30 58	23.3	0.16	0.13	0.38	17
6.	Terra Nova K-08	N 46 27 30	W 48 30 59	24.7	0.12	0.10	0.16	19
7.	Terra Nova K-17	N 46 26 43	W 48 32 32	24.3	0.16	0.15	0.32	20
8.	Terra Nova K-18	N 46 27 44	W 48 32 32	24.4	0.20	0.16	0.39	15

HIBERNIA WELLS

No.	Name and Symbol	Latitude	Longitude	KB (m)	[ρ_m (Ω.m)	ρ_{mf} (Ω.m)	ρ_{mc}] at (Ω.m)	T (°C)
1.	Hibernia B-08	N 46 47 06	W 48 45 30	25.9	0.41	0.38	0.48	15
2.	Hibernia B-27	N 46 46 10	W 48 48 28	27.1	0.38	0.31	0.55	25
3.	Hibernia C-96	N 46 45 10	W 48 44 36	33.2	0.06	0.06	0.22	18
4.	Hibernia K-14	N 46 43 40	W 48 47 36	33.2	0.07	0.06	0.13	21
5.	Hibernia K-18	N 46 47 34	W 48 47 17	29.7	0.34	0.27	0.39	24
6.	Hibernia P-15	N 46 44 59	W 48 46 51	15.0	0.29	0.20	0.49	17

Note: KB denotes Kelly bushing in m; ρ_m, ρ_{mf}, and ρ_{mc} (in Ω.m) denote, respectively, mud resistivity, mud filtrate resistivity, and mud cake resistivity. T is mean sample temperature in °C.

Table (2.1): Ranges of the log measurements used as input data to deduce various physical parameters.

TERRA NOVA WELLS

No.	SP(mv)	GR(API)	DEN(kg/m^3)	SON(μs/m)	CNL(%)	LL8(Ω.m.)	ILM(Ω.m.)	ILD(Ω.m.)	LLD(Ω.m.)	MLL(Ω.m.)	CALI(mm)
1.	----------	10 - 92	1863 - 2762	161 - 350	02 - 58	----------	1.4 - 452	1.3 - 0447	----------	----------	308 - 369
2.	----------	12 - 80	1615 - 2750	173 - 411	01 - 64	----------	1.2 - 493	1.1 - 1459	----------	----------	310 - 387
3.	-063 - -035	39 - 110	1348 - 2728	----------	04 - 55	----------	0.7 - 2021	1.0 - 2059	1.0 - 570	----------	----------
4.	-186 - -064	27 - 112	1958 - 2790	172 - 384	04 - 54	----------	0.8 - 2021	0.8 - 2011	1.2 - 478	----------	302 - 394
5.	-125 - -105	28 - 99	1518 - 3724	165 - 396	05 - 52	----------	0.8 - 2038	0.9 - 2132	----------	----------	303 - 333
6.	-274 - -049	36 - 98	1644 - 2668	----------	10 - 35	0.4 - 28	0.2 - 1948	0.7 - 2028	0.8 - 400	----------	----------
7.	-042 - -017	24 - 92	1533 - 2702	136 - 409	01 - 59	----------	0.5 - 1791	0.4 - 0122	----------	----------	249 - 376
8.	-164 - -136	23 - 98	1500 - 2696	136 - 495	07 - 43	----------	----------	----------	0.7 - 132	0.1 - 9871	233 - 488

HIBERNIA WELLS

No.	SP(mv)	GR(API)	DEN(kg/m^3)	SON(μs/m)	CNL(%)	LL8(Ω.m.)	ILM(Ω.m.)	ILD(Ω.m.)	LLD(Ω.m.)	MLL(Ω.m.)	CALI(mm)
1.	-124 - -26	08 - 79	2310 - 2818	161 - 445	03 - 48	1.6 - 0444	----------	1.2 - 0047	----------	----------	----------
2.	-064 - -28	16 - 117	2364 - 2724	133 - 660	05 - 44	0.9 - 0090	----------	0.2 - 0039	----------	----------	----------
3.	-052 - 12	16 - 107	2322 - 2728	177 - 332	05 - 44	0.9 - 1296	0.7 - 0913	0.8 - 0232	----------	----------	196 - 351
4.	-111 - -70	33 - 134	1497 - 3305	185 - 328	06 - 62	----------	0.3 - 2078	0.3 - 2000	----------	----------	----------
5.	-115 - 06	09 - 68	2258 - 2733	157 - 400	05 - 46	0.3 - 1433	----------	0.3 - 1890	----------	----------	----------
6.	-144 - -16	10 - 68	2203 - 2783	163 - 457	06 - 46	0.4 - 1387	----------	0.3 - 0078	----------	----------	----------

Note: (---------) denotes no data available.

Table (2.2): Average log values of the intervals examined.

TERRA NOVA WELLS

No.	SP(mv)	GR(API)	DEN(kg/m^3)	SON(μs/m)	CNL(%)	LL8(Ω.m.)	ILM(Ω.m.)	ILD(Ω.m.)	LLD(Ω.m.)	MLL(Ω.m.)	CALI(mm)
1.	------	49.4	2540	260	25.1	------	32.6	30.6	------	------	325
2.	------	48.5	2443	272	27.0	------	33.5	36.6	------	------	327
3.	-49	85.3	2353	-----	31.7	------	19.4	33.4	17.1	------	-----
4.	-116	82.6	2264	278	32.1	------	36.5	28.6	14.7	------	339
5.	-118	72.6	2258	280	31.7	------	28.5	66.5	------	------	326
6.	-158	72.9	2243	-----	24.3	1.17	12.6	22.7	13.9	------	-----
7.	-31	64.2	2264	274	32.6	------	06.1	03.8	------	------	327
8.	-158	63.9	2324	275	25.6	------	------	------	06.2	74.6	288

HIBERNIA WELLS

No.	SP(mv)	GR(API)	DEN(kg/m^3)	SON(μs/m)	CNL(%)	LL8(Ω.m.)	ILM(Ω.m.)	ILD(Ω.m.)	LLD(Ω.m.)	MLL(Ω.m.)	CALI(mm)
1.	-40	46.5	2636	251	22.9	12.5	------	05.2	------	------	-----
2.	-37	79.8	2584	263	27.6	04.2	------	02.4	------	------	-----
3.	-25	65.1	2577	252	22.7	15.0	06.0	05.8	------	------	-----
4.	-96	92.2	2480	235	19.9	------	73.1	51.1	------	------	224
5.	-25	42.3	2575	254	23.4	11.3	------	09.2	------	------	-----
6.	-71	38.2	2504	242	22.8	23.9	------	06.8	------	------	-----

Note: For Tables 2.1 and 2.2, SP denotes spontaneous potential log in mv; GR denotes gamma ray log in API units; DEN denotes bulk density log in kg/m^3; SON denotes transit time sonic log in μs/m; CNL denotes compensated neutron porosity log in %; LL8 denotes lateral resistivity log 8 in Ω.m; ILM denotes medium induction lateral resistivity log in Ω.m; ILD denotes deep induction lateral resistivity log in Ω.m; LLD denotes deep lateral resistivity log in Ω.m; MLL denotes micro-resistivity lateral log in Ω.m; and CALI denotes borehole diameter caliper log in mm.

Table (2.3): Selected values of transit time, compressional wave velocity and bulk density (modified after Bourbie et al., 1987).

Sediment or Rock Type	Transit Time (μs/m)	Comp. Velocity (m/s)	Bulk Density (gm/cm^3)
Dry sands	833 - 2500	400 - 1200	1.5 - 1.7
Wet sands	500 - 667	1500 - 2000	1.9 - 2.1
Saturated shales and clays	400 - 910	1100 - 2500	2.0 - 2.4
Marls	333 - 500	2000 - 3000	2.1 - 2.6
Saturated sands and shales	455 - 667	1500 - 2200	2.1 - 2.4
Porous and saturated sandstones	285 - 500	2000 - 3500	2.1 - 2.4
Limestone	166 - 285	3500 - 6000	2.4 - 2.7
Chalk	385 - 435	2300 - 2600	1.8 - 2.3
Rock salt	180 - 220	4500 - 5500	2.1 - 2.3
Anhydrite	180 - 250	4000 - 5500	2.9 - 3.0
Dolomite	150 - 285	3500 - 6500	2.5 - 2.9
Coal	370 - 455	2200 - 2700	1.3 - 1.8
Water	667 - 690	1450 - 1500	1.0 - 1.03
Ice	263 - 295	3400 - 3800	0.9
Oil	800 - 835	1200 - 1250	0.6 - 0.9
Oil saturated sands (20% porosity)	290	3440	1.8 - 1.9
Water saturated sands (20% porosity)	268	3736	1.8 - 1.9

Note: The values of the last two materials are taken from Schoen (1983).

Table (2.4): Empirical equations relating some of the log measurements (Fig. 2.1).

RELATED LOGS	FIGURE	EMPIRICAL EQUATION	*	**	***	EQUATION NO.
SP, ILD	(2.1-A)	$SP = -5.521*10^{+1} - 1.012$ ILD	$4.477*10^{+1}$	$1.810*10^{+1}$	$6.360*10^{-1}$	(2.1.1)
SON, DEN	(2.1-B)	$SON = 4.481*10^{+2} - 7.611*10^{-2}$ DEN	$1.070*10^{+1}$	$5.630*10^{+1}$	$2.290*10^{-2}$	(2.1.2)
CNL, SON	(2.1-C)	$CNL = -3.959*10^{+1} + 2.514*10^{-1}$ SON	$2.005*10^{0}$	$1.070*10^{+1}$	$4.090*10^{-2}$	(2.1.3)

Note: * Denotes mean absolute deviation (MAD) per point, ** denotes error in a coefficient, *** denotes error in b coefficient. SP in mv, ILD in Ω.m, SON in μs/m, DEN in kg/m^3 and CNL in %.

Table (2.5): Ranges of lithological composition and porosity of the various wells.

TERRA NOVA WELLS

No.	SH (%)	SS (%)	SILT (%)	LS (%)	MARL (%)	CGLM (%)	POR (%)
1.	0-53.2	0-68.0	5.8-40.5	0.4-42.0	----------	----------	0-23.6
2.	0-46.2	0-47.2	4.1-48.3	9.3-50.1	----------	5.1-42.5	0.7-31.8
3.	0-51.5	0-47.3	7.6-34.3	0.0-54.8	----------	----------	0-54.5
4.	0-39.2	0-35.4	2.1-33.6	2.4-31.9	1.7-33.7	----------	0-33.7
5.	0-63.2	4.3-67.4	7.0-96.4	0.0-43.1	----------	----------	0-41.2
6.	0-52.4	0-69.0	0.0-58.2	----------	----------	----------	0-46.8
7.	0-63.7	3.8-76.9	1.5-97.7	8.1-55.3	----------	17.3-39.4	0-38.5
8.	0-60.2	0-79.5	5.8-37.9	0.0-44.7	----------	----------	0-52.8

HIBERNIA WELLS

No.	SH (%)	SS (%)	SILT (%)	LS (%)	MARL (%)	CGLM (%)	POR (%)
1.	0-44.6	12.9-46.0	13.6-49.3	13.3-33.2	----------	----------	0-38.9
2.	0-44.7	0.0-73.1	11.2-40.9	0.0-53.5	----------	----------	0-58.8
3.	0-43.5	0.0-43.5	5.9-36.0	2.7-39.6	----------	----------	9.2-25.9
4.	3.9-48.9	0.0-63.8	13.3-41.9	----------	----------	----------	0-35.7
5.	0-48.5	6.2-39.8	11.0-37.2	0.0-44.1	----------	----------	0-29.6
6.	0-54.0	0.0-44.9	2.1-41.4	7.6-36.5	----------	----------	0-52.3

Table (2.6): Averages of lithological composition and porosity of the various wells.

TERRA NOVA WELLS

No.	SH (%)	SS (%)	SILT (%)	LS (%)	MARL (%)	CGLM (%)	POR (%)
1.	23.2	25.6	23.0	19.2	------	------	09.7
2.	22.2	20.2	19.7	27.0	------	24.4	13.4
3.	27.0	20.3	23.7	21.1	------	------	11.2
4.	23.5	13.2	23.1	13.8	15.3	------	14.1
5.	31.7	31.1	27.6	16.7	------	------	16.7
6.	31.7	34.7	18.3	-----	------	------	15.4
7.	23.0	30.6	28.4	23.2	------	29.2	18.2
8.	24.4	25.5	25.5	22.3	------	------	16.8

HIBERNIA WELLS

No.	SH (%)	SS (%)	SILT (%)	LS (%)	MARL (%)	CGLM (%)	POR (%)
1.	20.8	25.4	25.2	22.3	------	------	10.3
2.	27.9	26.1	26.5	13.8	------	------	13.7
3.	22.7	19.1	22.4	19.6	------	------	16.3
4.	28.5	27.7	29.8	------	------	------	14.0
5.	25.5	21.7	25.9	19.4	------	------	07.5
6.	22.2	26.6	26.3	22.5	------	------	13.5

Note: For Tables 2.5 and 2.6, SH, SS, SILT, LS, MARL and CGLM denote, respectively, fractions (in %) of shale, sandstone, silt, limestone, marl and conglomerate; POR = Φ denotes porosity in %; and ----- denotes no data available.

Table (2.7): Ranges and averages of shale content (VSH) and permeability (K) in mD and m^2.

TERRA NOVA WELLS

No.	VSH (%)	$\overline{VSH}$ (%)	K (mD)	$\overline{K}$ (mD)	K (m^2)	$\overline{K}$ (m^2)
1.	0.2 - 95.0	32.0	0.1 - 08976	276	$9.87*10^{-17}$ - $8.86*10^{-12}$	$2.72*10^{-13}$
2.	0.5 - 99.9	38.6	0.1 - 32405	695	$9.87*10^{-17}$ - $3.20*10^{-11}$	$6.86*10^{-13}$
3.	1.0 - 93.1	48.2	0.1 - 58818	649	$9.87*10^{-17}$ - $5.81*10^{-11}$	$6.41*10^{-13}$
4.	1.1 - 91.8	47.1	0.1 - 22060	085	$9.87*10^{-17}$ - $2.18*10^{-11}$	$8.39*10^{-14}$
5.	0.2 - 93.8	45.5	0.1 - 07218	039	$9.87*10^{-17}$ - $7.12*10^{-12}$	$3.85*10^{-14}$
6.	0.8 - 92.3	43.7	0.1 - 18824	400	$9.87*10^{-17}$ - $1.86*10^{-12}$	$3.95*10^{-13}$
7.	0.9 - 95.5	44.6	0.1 - 01619	017	$9.87*10^{-17}$ - $1.60*10^{-12}$	$1.68*10^{-14}$
8.	0.4 - 93.1	38.2	0.1 - 10997	052	$9.87*10^{-17}$ - $1.09*10^{-12}$	$5.13*10^{-14}$

HIBERNIA WELLS

No.	VSH (%)	$\overline{VSH}$ (%)	K (mD)	$\overline{K}$ (mD)	K (m^2)	$\overline{K}$ (m^2)
1.	1.1 - 94.1	36.9	0.1 - 13132	046	$9.87*10^{-17}$ - $1.30*10^{-11}$	$4.54*10^{-14}$
2.	0.3 - 92.3	44.2	0.1 - 68812	081	$9.87*10^{-17}$ - $6.79*10^{-11}$	$8.00*10^{-14}$
3.	0.5 - 96.7	37.8	0.6 - 01360	029	$5.92*10^{-16}$ - $1.34*10^{-12}$	$2.86*10^{-14}$
4.	0.1 - 96.3	42.2	0.1 - 151817	619	$9.87*10^{-17}$ - $1.50*10^{-10}$	$6.11*10^{-13}$
5.	1.2 - 90.2	37.7	0.1 - 28871	099	$9.87*10^{-17}$ - $2.85*10^{-11}$	$9.77*10^{-14}$
6.	0.4 - 91.9	32.7	0.1 - 28757	279	$9.87*10^{-17}$ - $2.84*10^{-11}$	$2.75*10^{-13}$

Note: VSH and $\overline{VSH}$ denote, respectively, volume of shale and silt combined and its average in %; K and $\overline{K}$ (in mD and m^2) denote, respectively, permeability and average permeability, 1 mD equals $9.87*10^{-16}$ m^2.

Table (2.8): Empirical equations relating porosity (Φ), permeability (K) and litological fractions (Fig. 2.2).

FRACTION	FIGURE	EMPIRICAL EQUATION		MAD	a ERROR	b ERROR	EQUATION NO.
SHALE	(2.2-A)	$\Phi = 8.908 + 1.865*10^{-1}$	SH	3.102	6.23	$2.44*10^{-1}$	(2.2.1.2.2)
	(2.2-B)	$K = -6.917*10^{+1} + 1.223*10^{+1}$	SH	$2.58*10^{+2}$	$5.18*10^{+2}$	$2.03*10^{+1}$	(2.2.1.2.3)
SANDSTONE	(2.2-C)	$\Phi = 9.222 + 1.774*10^{-1}$	SS	3.005	3.80	$1.49*10^{-1}$	(2.2.1.2.4)
	(2.2-D)	$K = 2.852*10^{+2} - 1.80166$	SS	$2.62*10^{+2}$	$3.31*10^{-2}$	$1.30*10^{+1}$	(2.2.1.2.5)
SILTSTONE	(2.2-E)	$\Phi = 1.120*10^{+1} + 9.835*10^{-2}$	SILT	3.159	6.79	$2.73*10^{-1}$	(2.2.1.2.6)
	(2.2-F)	$K = 8.209*10^{+2} - 2.353*10^{+1}$	SILT	$2.50*10^{+2}$	$5.37*10^{+2}$	$2.16*10^{+1}$	(2.2.1.2.7)
LIMESTONE	(2.2-G)	$\Phi = 1.319*10^{+1} + 1.255*10^{-2}$	LS	3.426	5.43	$2.66*10^{-1}$	(2.2.1.2.8)
	(2.2-H)	$K = -3.675*10^{+2} + 2.833*10^{+1}$	LS	$2.31*10^{+2}$	$3.86*10^{+2}$	$1.86*10^{+1}$	(2.2.1.2.9)

Note: Φ in %, K in mD, SH, SS, SILT, and LS fractions in %.

Table (2.9): Ranges of the deduced electric parameters.

TERRA NOVA WELLS

No.	ρ_w (Ω.m)	S_w (%)	F	m	T	S_p (1/cm)	GSD (μm)
			(D I M E N S I O N L E S S)				
1.	0.001-12.1	32.6-100	14.5-187365	0.7-6.3	0.9-20.9	243-10801	5.1-198
2.	0.001-47.0	14.3-100	7.6-009066	1.3-7.1	1.6-08.1	106-11252	4.9-453
3.	0.001-315	0.70-100	2.4-029787	0.6-12.6	0.6-12.8	037-11243	4.9-1036
4.	0.001-71.7	1.80-100	6.7-036639	1.3-6.9	1.0-13.2	140-11205	5.0-349
5.	0.001-77.4	2.60-100	4.4-413734	1.0-6.2	1.0-28.8	198-11248	4.9-249
6.	0.001-03.1	2.40-100	3.2-075616	0.5-6.7	1.0-13.4	0.50-11856	2.7-4940
7.	0.001-0.76	25.5-100	5.1-002547	0.8-4.4	1.0-07.1	1354-11196	5.0-44
8.	0.001-8.00	8.50-100	2.6-131616	0.6-6.3	1.0-14.3	394-11219	4.9-151

HIBERNIA WELLS

No.	ρ_w (Ω.m)	S_w (%)	F	m	T	S_p (1/cm)	GSD (μm)
			(D I M E N S I O N L E S S)				
1.	0.001-5.20	5.5-100	5.00-22153	0.002-5.9	1.00-11.1	342-11223	4.9-150
2.	0.001-1.04	11-100	2.00-2641	1.33-9.7	1.00-4.6	507-11171	5.0-059
3.	0.035-2.98	8.3-100	11.9-110	1.35-4.0	1.75-3.2	655-6845	8.0-071
4.	0.001-120.6	1.1-100	6.00-6957	0.90-8.4	1.00-9.6	73-11177	5.0-623
5.	0.001-26.03	1.0-100	9.00-47537	0.002-4.9	0.30-15.4	127-7728	7.3-419
6.	0.001-75.00	5.3-100	0.65-67209	0.690-6.6	0.37-10.7	367-1571108	0.04-120

Table (2.10): Averages of the electric deduced parameters.

TERRA NOVA WELLS

No.	ρ_w (Ω.m)	S_w (%)	F	m	T	S_p (1/cm)	GSD (μm)
			(D I M E N S I O N L E S S)				
1.	0.72	60.7	2172	2.74	3.80	3640	34.7
2.	1.32	46.3	0105	3.13	2.76	4233	35.3
3.	1.15	65.1	1162	2.72	3.23	3911	29.8
4.	0.38	59.4	0144	2.57	2.68	5050	14.1
5.	0.45	70.5	0875	2.36	2.65	5481	12.8
6.	0.21	53.4	0475	2.48	2.68	3557	18.8
7.	0.08	83.1	0055	2.08	2.27	6520	08.1
8.	0.18	76.5	0573	2.28	2.51	6016	11.1

HIBERNIA WELLS

No.	ρ_w (Ω.m)	S_w (%)	F	m	T	S_p (1/cm)	GSD (μm)
			(D I M E N S I O N L E S S)				
1.	0.07	52.4	451	2.06	3.38	4418	15.5
2.	0.05	62.4	075	2.55	2.63	5488	11.5
3.	0.15	45.6	037	2.04	2.33	3613	15.4
4.	1.20	41.1	073	3.08	2.60	3552	26.7
5.	0.06	42.0	847	1.59	4.00	3454	24.0
6.	0.53	55.8	541	2.17	2.11	25736	11.5

Note: For Tables 2.9 and 2.10, ρ_w denotes pore water resistivity in Ω.m; S_w denotes water saturation in %; m denotes dimensionless cementation factor; F denotes dimensionless formation resistivity factor; T denotes dimensionless tortuosity; S_p denotes specific internal surface area in cm^{-1}; GSD denotes distribution of mean grain size in μm.

Table (2.11): Empirical equations of the plots in Figures 2.4 and 2.5 showing relationships between the deduced petrophysical and electric parameters, and the log measured parameters.

FIGURE	EMPIRICAL EQUATION	*	**	***	EQUATION No.
(2.4-A)	$T = 5.034 - 1.617*10^{-1}\ \Phi$	$2.839*10^{-1}$	$3.60*10^{-1}$	$2.58*10^{-2}$	(2.2.2.6.1)
(2.4-B)	$T = 3.225 - 1.632*10^{-1}\ m$	$5.824*10^{-1}$	$9.34*10^{-1}$	$3.81*10^{-1}$	(2.2.2.6.2)
(2.4-C)	$T = 2.804 + 5.677*10^{-2}\ \rho_w$	$5.862*10^{-1}$	$2.29*10^{-1}$	$3.57*10^{-1}$	(2.2.2.6.3)
(2.4-D)	$T = 3.565 - 1.263*10^{-2}\ S_w$	$5.625*10^{-1}$	$7.30*10^{-1}$	$1.23*10^{-2}$	(2.2.2.6.4)
(2.4-E)	$\rho_o = 18.87 + 8.175*10^{-3}\ F$	$2.049*10^{+1}$	$7.70*10^{0}$	$9.62*10^{-3}$	(2.2.2.6.5)
(2.4-F)	$D = 15.28 + 7.375*10^{-3}\ F$	$8.482*10^{0}$	$3.13*10^{0}$	$3.98*10^{-3}$	(2.2.2.6.6)
(2.4-G)	$\Phi = 15.10 - 2.720*10^{-3}\ F$	$2.700*10^{0}$	$9.96*10^{-1}$	$1.27*10^{-3}$	(2.2.2.6.7)
(2.4-H)	$K = 219.2 + 3.917*10^{-2}\ F$	$2.608*10^{-2}$	$9.62*10^{+1}$	$1.22*10^{-1}$	(2.2.2.6.8)
(2.5-A)	$\Phi = 17.37 - 1.941*10^{-1}\ D$	$2.576*10^{0}$	$1.65*10^{0}$	$7.76*10^{-2}$	(2.2.2.6.9)
(2.5-B)	$K = -160.77 + 2.084*10^{+1}\ D$	$1.696*10^{+2}$	$1.08*10^{+2}$	$5.11*10^{0}$	(2.2.2.6.10)
(2.5-C)	$T = 2.135 + 3.614*10^{-2}\ D$	$4.739*10^{-1}$	$3.03*10^{-1}$	$1.43*10^{-2}$	(2.2.2.6.11)
(2.5-D)	$S_p = 10.40 - 2.264*10^{-1}\ D$	$5.589*10^{0}$	$3.58*10^{0}$	$1.69*10^{-1}$	(2.2.2.6.12)
(2.5-E)	$SP = -88.46 + 6.899*10^{-1}\ D$	$5.268*10^{+1}$	$4.15*10^{+1}$	$2.32*10^{0}$	(2.2.2.6.13)
(2.5-F)	$ILD = 5.661 + 9.560*10^{-1}\ D$	$1.868*10^{+1}$	$1.19*10^{+1}$	$5.63*10^{-1}$	(2.2.2.6.14)
(2.5-G)	$GR = 67.40 - 1.482*10^{-1}\ D$	$1.795*10^{+1}$	$1.15*10^{+1}$	$5.41*10^{-1}$	(2.2.2.6.15)
(2.5-H)	$DEN = 2365 + 3.470*10^{0}\ D$	$1.451*10^{+2}$	$9.27*10^{+1}$	$4.37*10^{0}$	(2.2.2.6.16)

Note: * Denotes mean absolute deviation per point; ** denotes error in a coefficient; *** denotes error in b coefficient; T, F, and m are dimensionless parameters; Φ and S_w are in %; K in mD, S_p in cm^{-1} should be multiplied by 1000; D = GSD = grain size diameter in µm; ρ_o = ILD; ρ_o and ρ_w are in Ω.m; SP in mv; GR in API; DEN in kg/m^3.

Table (2.12): Ranges of elastic properties derived from compressional wave velocity, bulk density and shale content.

TERRA NOVA WELLS

No.	σ	(V_p) [m/s]	$(V_p)^2$ [km/s]^2	(V_p / V_s)	(V_s) [m/s]	$(V_s)^2$ [km/s]^2	μ[GPa]	*K*[GPa]	β/100 [GPa]$^{-1}$	(K/μ)	E[GPa]	λ[GPa]	Γ [(km/s)*(gm/cm^3)]
1.	0.2703-0.3887	2862-6175	8.2-38.1	1.78-2.34	1433-3445	2.1-11.9	4.21-32.77	10.68-61.62	1.62-09.37	1.84-4.16	11.17-83.50	7.87-39.77	5.5-17.1
2.	0.2706-0.3948	2435-5755	5.9-33.1	1.78-2.40	1227-3220	1.5-10.4	2.98-27.92	08.54-51.97	1.92-11.72	1.85-4.42	08.27-71.03	6.36-33.36	5.0-15.5
3.	0.2712-0.3863	----------	----------	----------	----------	----------	----------	----------	----------	----------	----------	----------	----------
4.	0.2713-0.3848	2605-5785	6.8-33.5	1.78-2.31	1167-3230	1.4-10.4	3.09-27.91	11.29-52.31	1.91-08.82	1.85-4.01	08.51-71.08	7.76-34.35	5.9-15.5
5.	0.2703-0.3873	2526-6050	6.4-36.6	1.78-2.33	1201-3294	1.5-10.9	2.90-25.08	09.23-51.15	1.96-11.08	1.84-4.10	08.05-64.66	6.71-34.44	5.0-14.3
6.	0.2710-0.3854	----------	----------	----------	----------	----------	----------	----------	----------	----------	----------	----------	----------
7.	0.2711-0.3894	2447-7352	5.9-54.1	1.78-2.35	1142-3658	1.3-13.4	2.23-27.32	07.25-73.15	1.37-13.79	1.85-4.19	06.06-72.23	5.78-55.12	4.1-15.0
8.	0.2705-0.3864	2021-7354	4.8-54.1	1.78-2.32	1037-4006	1.1-16.0	1.71-40.96	04.20-83.44	1.19-23.82	1.85-4.08	04.51-105.6	3.06-56.14	3.2-18.8

HIBERNIA WELLS

No.	σ	(V_p) [m/s]	$(V_p)^2$ [km/s]^2	(V_p / V_s)	(V_s) [m/s]	$(V_s)^2$ [km/s]^2	μ[GPa]	*K*[GPa]	β/100 [GPa]$^{-1}$	(K/μ)	E[GPa]	λ[GPa]	Γ [(km/s)*(gm/cm^3)]
1.	0.2713-0.3876	2251-6175	5.0-38.2	1.78-2.33	1178-3239	1.4-10.5	3.53-28.58	08.18-67.56	1.48-12.23	1.85-4.11	09.26-75.14	05.83-48.50	5.7-17.1
2.	0.2703-0.3854	1515-7510	2.3-56.4	1.78-2.32	0775-3583	0.6-12.8	1.56-32.40	03.87-99.13	1.01-25.85	1.84-4.03	04.12-87.66	02.83-77.53	3.9-19.0
3.	0.2706-0.3909	3013-5632	9.1-31.7	1.78-2.36	1369-3152	01.9-9.9	4.82-26.17	15.97-48.61	2.06-06.26	1.85-4.25	13.20-66.56	12.12-31.17	7.6-14.8
4.	0.2702-0.3904	3045-5395	9.3-29.1	1.78-2.36	1447-2802	02.1-7.9	4.17-19.95	14.27-47.35	2.11-07.01	1.84-4.23	11.41-52.48	10.90-34.1	5.5-14.2
5.	0.2715-0.3827	2505-6370	6.3-40.6	1.79-2.29	1274-3406	1.6-11.6	3.93-29.34	09.94-63.50	1.57-10.06	1.89-3.93	10.41-76.28	07.32-43.94	6.0-16.2
6.	0.2705-0.3849	2188-6121	4.8-37.5	1.78-2.31	1050-3292	1.1-10.8	2.67-29.81	07.33-61.69	1.62-13.65	1.85-4.01	07.22-77.03	05.43-41.82	5.0-16.8

Table (2.13): Averages of elastic properties derived from compressional wave velocity, bulk density and shale content, with the same dimensions given in Table 2.12.

TERRA NOVA WELLS

No.	σ	(V_p)	$(V_p)^2$	(V_p / V_s)	(V_s)	$(V_s)^2$	μ	*K*	β/100	(*K*/μ)	E	λ	Γ
1.	0.310	3923	15.7	1.91	2061	4.4	11.17	25.21	4.29	2.34	29.13	17.77	10.0
2.	0.318	3742	14.3	1.95	1935	3.9	09.55	22.53	4.86	2.49	25.03	16.16	09.2
3.	0.330	------	-----	-----	------	----	------	-------	-----	-----	-------	------	-----
4.	0.329	3678	13.9	1.99	1863	3.6	09.02	22.46	4.84	2.64	23.79	16.45	09.1
5.	0.327	3649	13.6	1.98	1854	3.6	08.20	20.18	5.43	2.62	21.61	14.71	08.3
6.	0.325	------	-----	-----	------	----	------	-------	-----	-----	-------	-------	----
7.	0.326	3758	14.6	1.99	1916	3.9	09.02	21.66	5.21	2.63	23.65	15.64	08.6
8.	0.318	3754	14.6	1.95	1945	4.0	09.58	22.24	5.13	2.48	25.04	15.85	09.0

HIBERNIA WELLS

No.	σ	(V_p)	$(V_p)^2$	(V_p / V_s)	(V_s)	$(V_s)^2$	μ	*K*	β/100	(*K*/μ)	E	λ	Γ
1.	0.316	4056	16.7	1.94	2104	4.5	11.96	28.41	3.78	2.43	31.40	20.44	10.7
2.	0.325	3846	15.0	1.97	1959	3.9	10.09	25.18	4.10	2.57	26.65	18.46	09.9
3.	0.317	4010	16.3	1.94	2076	4.4	11.36	26.81	3.86	2.46	29.78	19.24	10.4
4.	0.323	4264	18.2	1.97	2174	4.8	11.83	29.59	3.47	2.55	31.22	21.71	10.6
5.	0.317	3985	16.1	1.94	2061	4.3	11.12	26.51	3.94	2.44	29.21	19.10	10.3
6.	0.311	4238	18.4	1.92	2221	5.1	12.88	29.19	3.79	2.38	33.58	20.61	10.7

Table (2.14): Compressional and shear wave velocities, and velocity ratios (after Pickett, 1963 and Gregory, 1977).

SUBSTANCE	V_p (m/s) (*)	V_s (m/s) (*)	V_p / V_s (**)
Brine saturated sandstone	2393-3962	1097-2426	2.18-1.63
Oil saturated sandstone	2249-3956	1116-2448	2.02-1.62
Gas saturated sandstone	1811-3798	1207-2533	1.50
Brine saturated shale	2500-3703		(***)
Sandstones	5486-5944		1.65-1.75
Limestones	6400-7010		1.85-1.95
Dolomites	7010-7315		1.75-1.85

Note: V_p denotes compressional wave velocity; V_s denotes shear wave velocity; and V_p / V_s denotes velocity ratio. The saturated sandstones correspond to porosity values between 34.6 and 17.8% and density values between 1.71 and 2.35 gm/cm^3 at depth between 1220 and 5182 m. Brine saturated shale corresponds to porosity values between 27 and 15.3% and a range of density between 2.24 and 2.43 gm/cm^3. (*) Denotes data after Gregory (1977); (**) denotes values calculated from V_p and V_s; and (***) denotes data after Pickett (1963). Pickett's data relate to a confining pressure between 0 and $4.1*10^7$ Pa.

Table (2.15): Values of some of the elastic moduli for different substances (after Clark, 1966 and Gregory, 1977).

SUBSTANCE (*)	μ (GPa)	SUBSTANCE (**)	*K* (GPa)	SUBSTANCE (**)	*K* (GPa)	SUBSTANCE (*)	$\beta*10^{-12}$ 1/GPa(*)	SUBSTANCE	E (GPa)
Shales and siltstones	12-16	Quartz	38	Distilled water	2.239	Dolomite	1.49-1.72	Limestone	53-079
Limestones	20-30	Calcite	67	Sea Water	2.402	Sandstone	2.33-4.83	Dolomite	71-093
Dolomites	32-42	Anhydrite	54	Brine	2.752			Sandstone	40-100
Sandstones	17-47	Dolomite	82	Crude oil	0.862			Dry shale	23-044
		Halite	23	Crude oil	1.740			Wet shale	19
		Gypsum	40						

Note: The bulk modulus (*K*) of the fluids was measured at 25°C; densities, in gm/cm^3, of distilled water, sea water, brine, crude oil are, respectively, 0.998, 1.025, 1.069, 0.85 and 0.80. (*) Denotes data after Clark (1966); (**) denotes data after Gregory (1977).

Table (2.16): Empirical equations relating various elastic, petrophysical and electric parameters and their Mean Absolute Deviation (MAD) and errors in a and b coefficients (Figures 2.6 and 2.7).

FIGURE	EMPERICAL EQUATION	MAD	a ERROR	b ERROR	EQUATION No.
(2.6-A L)	$VSH = 9.036*10^{+1} - 1.294*10^{-2}\ V_p$	4.325	$2.46*10^{+1}$	$6.30*10^{-3}$	(2.2.3.8.1)
(2.6-A R)	$S_p = 2.016*10^{+1} - 3.990*10^{-3}\ V_p$	$8.327*10^{-1}$	5.44	$1.40*10^{-3}$	(2.2.3.8.2)
(2.6-B L)	$V_s = -2.005*10^{+2} + 5.666*10^{-1}\ V_p$	$2.327*10^{+1}$	$1.33*10^{+2}$	$3.39*10^{-2}$	(2.2.3.8.3)
(2.6-B R)	$\Phi = 3.611*10^{+1} - 5.737*10^{-3}\ V_p$	3.106	$1.77*10^{+1}$	$4.52*10^{-3}$	(2.2.3.8.4)
(2.6-C L)	$K = -3.290*10^{+1} + 1.481*10^{-2}\ V_p$	$8.424*10^{-1}$	4.80	$1.23*10^{-3}$	(2.2.3.8.5)
(2.6-C R)	$S_w = 2.115*10^{+2} - 3.929*10^{-2}\ V_p$	$1.139*10^{+1}$	$6.49*10^{+1}$	$1.66*10^{-2}$	(2.2.3.8.6)
(2.7-A L)	$\beta = 2.8147 + 1.153*10^{-1}\ \Phi$	$5.837*10^{-1}$	$7.73*10^{-1}$	$5.52*10^{-2}$	(2.2.3.8.7)
(2.7-A R)	$\sigma = 3.103*10^{-1} + 7.717*10^{-4}\ \Phi$	$6.220*10^{-3}$	$7.88*10^{-3}$	$5.65*10^{-4}$	(2.2.3.8.8)
(2.7-B L)	$\sigma = -1.329*10^{-1} + 2.316*10^{-1}\ V_p / V_s$	$1.217*10^{-3}$	$2.75*10^{-2}$	$1.41*10^{-2}$	(2.2.3.8.9)
(2.7-B R)	$K/\mu = -4.8537 + 3.764\ V_p / V_s$	$1.001*10^{-2}$	$2.26*10^{-1}$	$1.16*10^{-1}$	(2.2.3.8.10)
(2.7-C L)	$(V_p)^2 = 1.76302 + 3.30214\ (V_s)^2$	$3.367*10^{-1}$	$9.10*10^{-1}$	$2.16*10^{-1}$	(2.2.3.8.11)
(2.7-C R)	$\Gamma = 3.06716 + 1.58871\ (V_s)^2$	$4.380*10^{-1}$	1.18	$2.81*10^{-1}$	(2.2.3.8.12)

Note: For Tables 2.12-2.16, VSH denotes shale content in %; V_p denotes compressional wave velocity in m/s; S_p denotes specific surface area of grains in cm^{-1}; V_s denotes shear wave velocity in m/s; Φ denotes porosity in %; K denotes bulk modulus in GPa; S_w denotes water saturation in %; β denotes bulk compressibility/100.0 in $(GPa)^{-1}$; σ denotes dimensionless Poisson's ratio; V_p/V_s denotes compressional to shear wave velocity ratio; μ denotes shear modules in GPa; E denotes Young's modulus in GPa; λ denotes Lame's constant in GPa; K/μ denotes bulk to shear moduli ratio; $(V_p)^2$ denotes square of compressional wave velocity in $(km/s)^2$; $(V_s)^2$ denotes square of shear wave velocity in $(km/s)^2$; and Γ denotes acoustic impedance in $[(km/s)*(gm/cm^3)]$. MAD denotes mean absolute deviation per point from the regression lines.

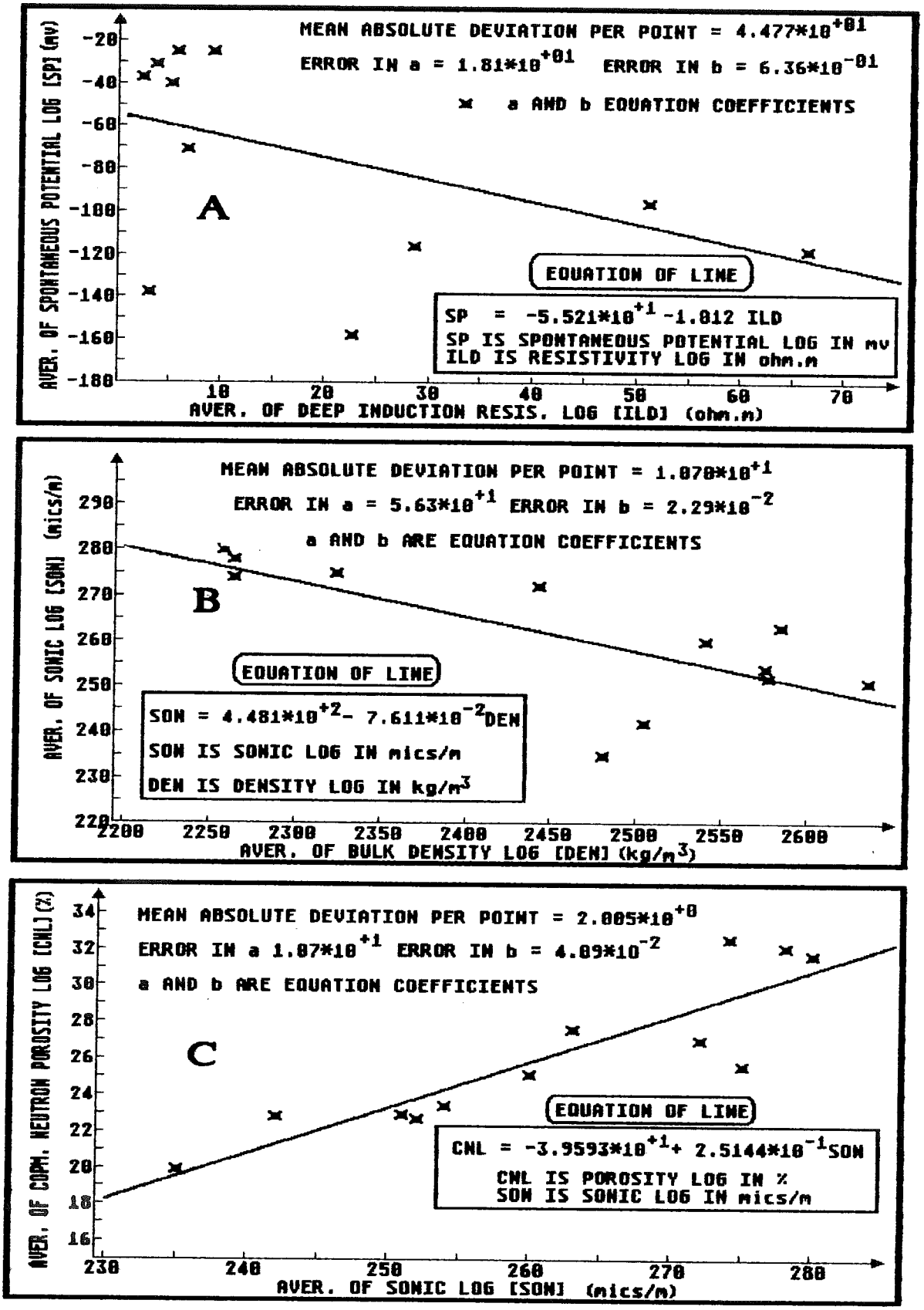

FIGURE (2.1): Relationships representing average log values for the Jeanne d'Arc Basin (JDB) at Terra Nova and Hibernia of resistivity and spontaneous potential logs (A); density and sonic logs (B); sonic and neutron porosity logs (C).

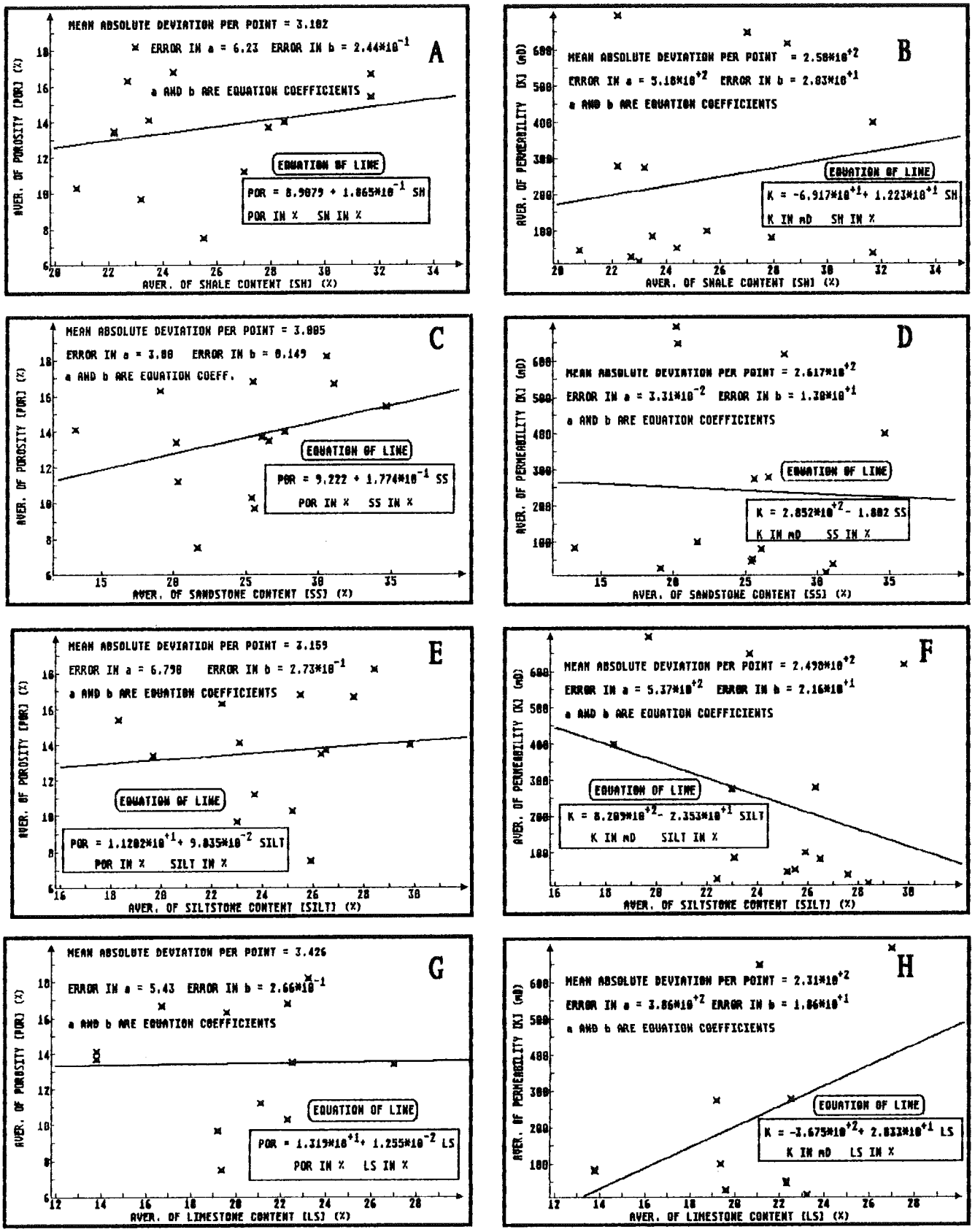

FIGURE (2.2): Various relationships (A to H) between porosity, permeability, and lithology fractions (shale, sandstone, silt, and limestone). The plotted data are the average values given in Tables 2.6 and 2.7.

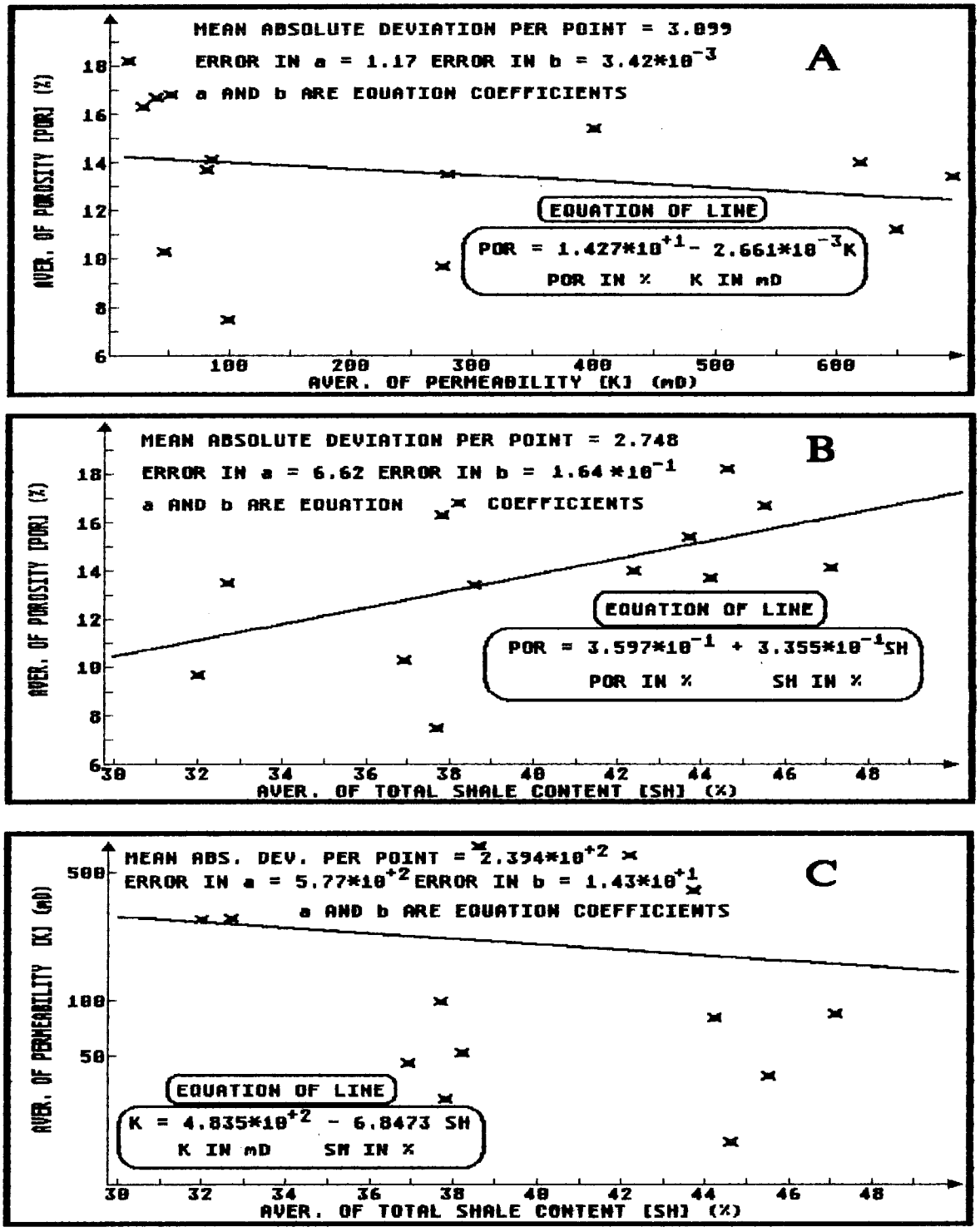

FIGURE (2.3): Relationships between porosity and permeability for all fractions combined (A); between porosity and total shale fraction (B); between permeability and total shale fraction (C).

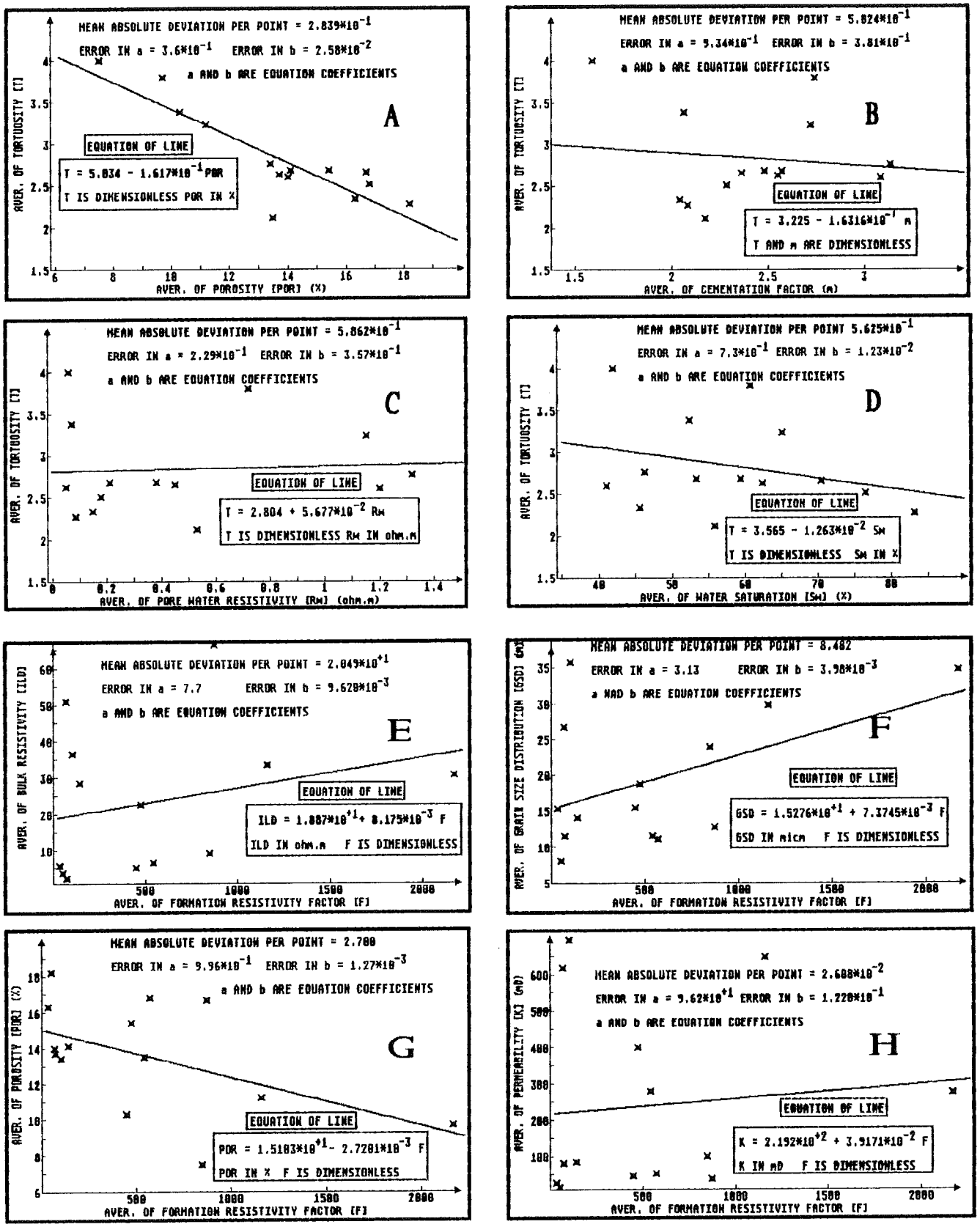

FIGURE (2.4): Relationships of tortuosity with porosity (A), cementation factor (B), pore water resistivity (C), and water saturation (D); and of formation factor with bulk resistivity (E), mean grain size distribution (F), porosity (G), and permeability (H).

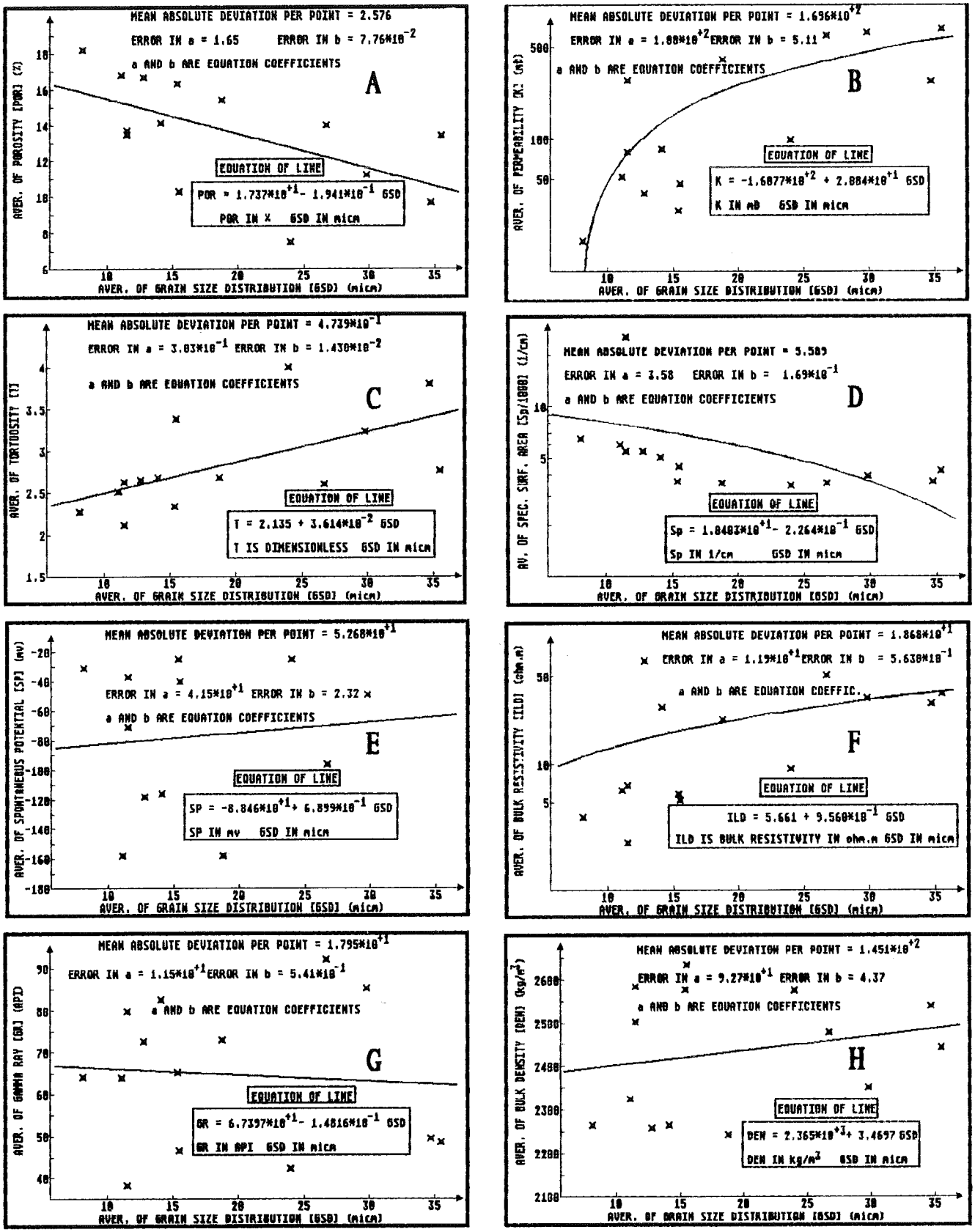

FIGURE (2.5): Relationships of mean grain size distribution (grain diameter) with porosity (A), permeability (B), tortuosity (C), specific surface area (D), spontaneous potential (E), bulk resistivity (F), gamma ray (G), and bulk density (H).

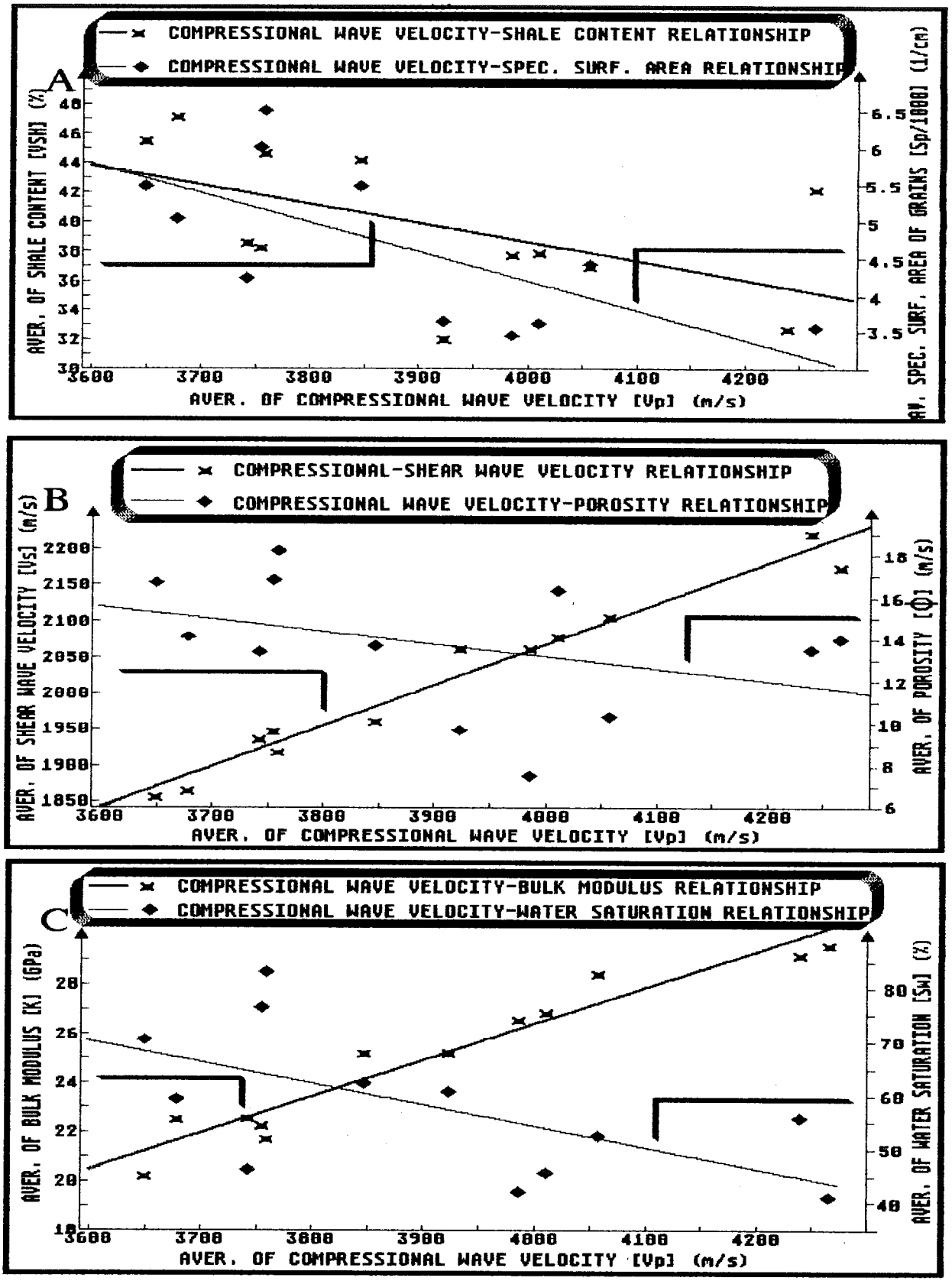

FIGURE (2.6): Relationships between compressional wave velocity and shale content (A-left), specific surface area of grains (A-right), shear wave velocity (B-left), porosity (B-right), bulk modulus (C-left), and water saturation (C-right).

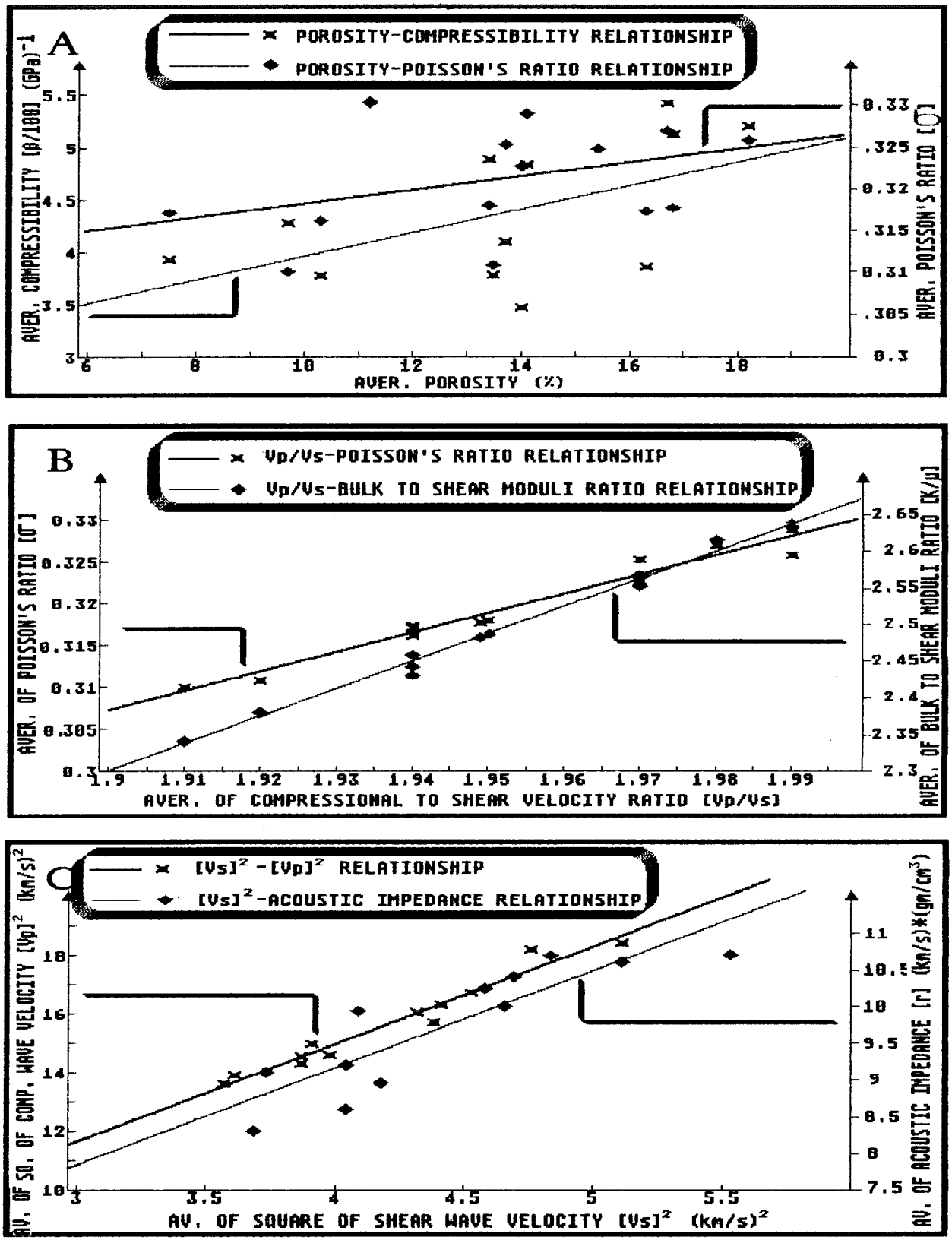

FIGURE (2.7): Relationships of porosity-compressibility (A-left) and porosity-Poisson's ratio (A-right); compressional to shear wave velocity ratio-Poisson's ratio (B-left), compressional to shear wave velocity ratio-bulk to shear modulus ratio (B-right); square of shear wave velocity-square of compressional wave velocity (C-left), and square of compressional wave velocity-acoustic impedance (C-right).

A: TERRA NOVA WELL C-09

B: TERRA NOVA WELL E-79

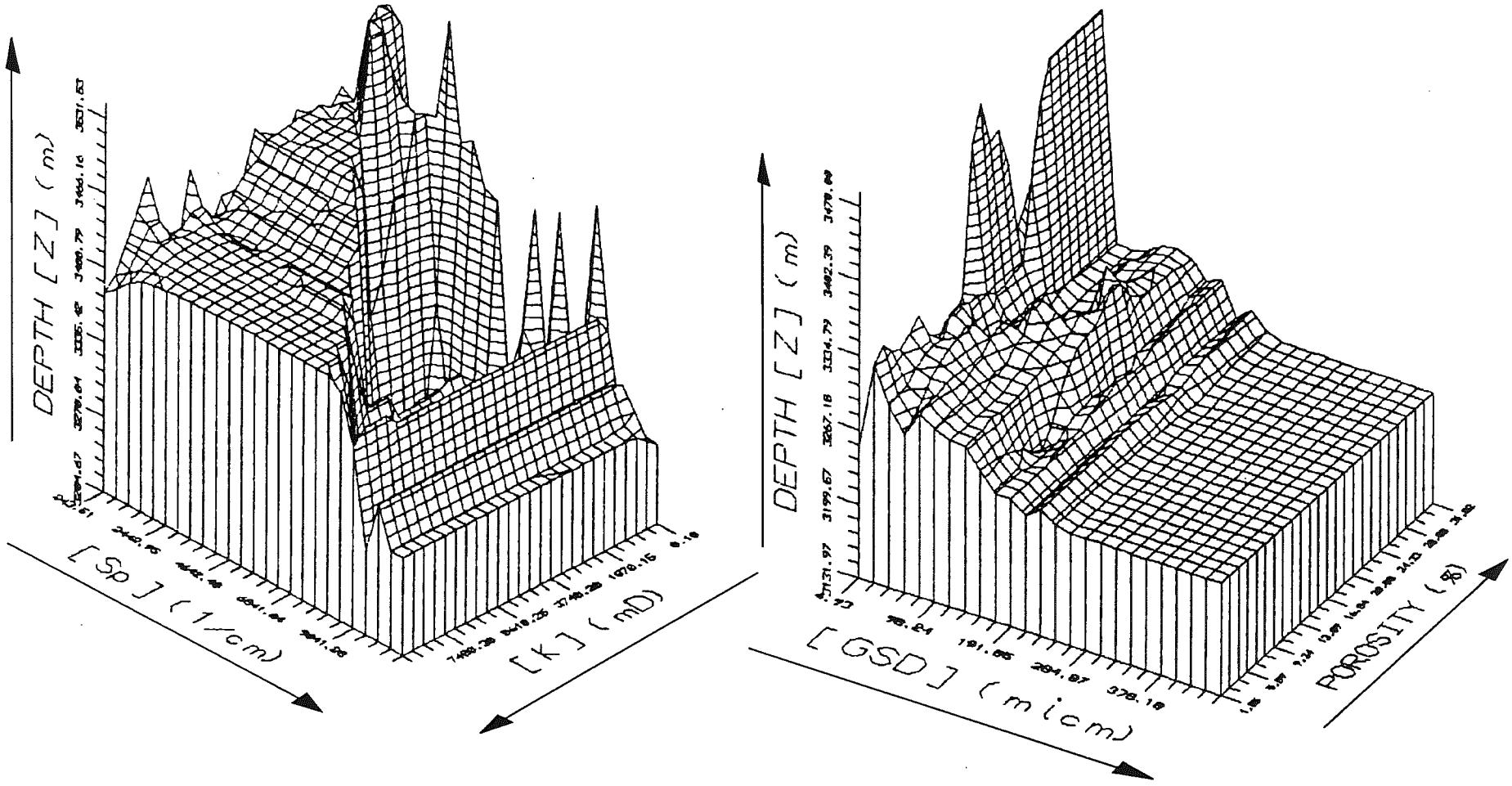

FIGURE (3.1): Three dimensional plots for the Terra Nova oil field; Permeability [K] - specific surface area [S_P] - depth [Z] for well C-09 (A); porosity [Φ] - mean size grain distribution [GSD] - depth [Z] for well E-79 (B).

C: TERRA NOVA WELL H-99

D: TERRA NOVA WELL I-97

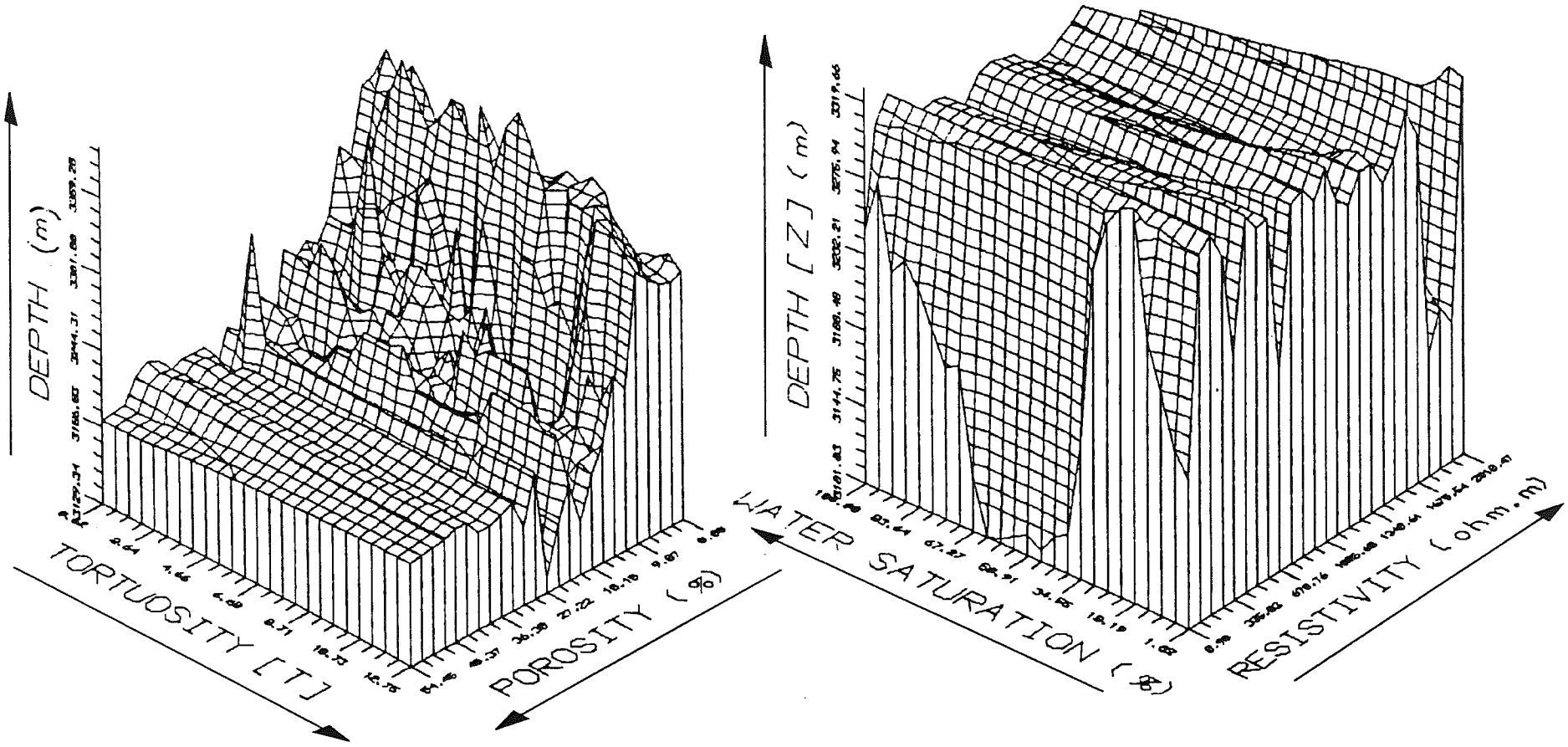

FIGURE (3.1) (cont'd): Porosity [Φ] - tortuosity [T] - depth [Z] for well H-99 (C); bulk resistivity [ILD] - water saturation [Sw] - depth [Z] for well I-97 (D).

E: TERRA NOVA WELL K-07

F: TERRA NOVA WELL K-08

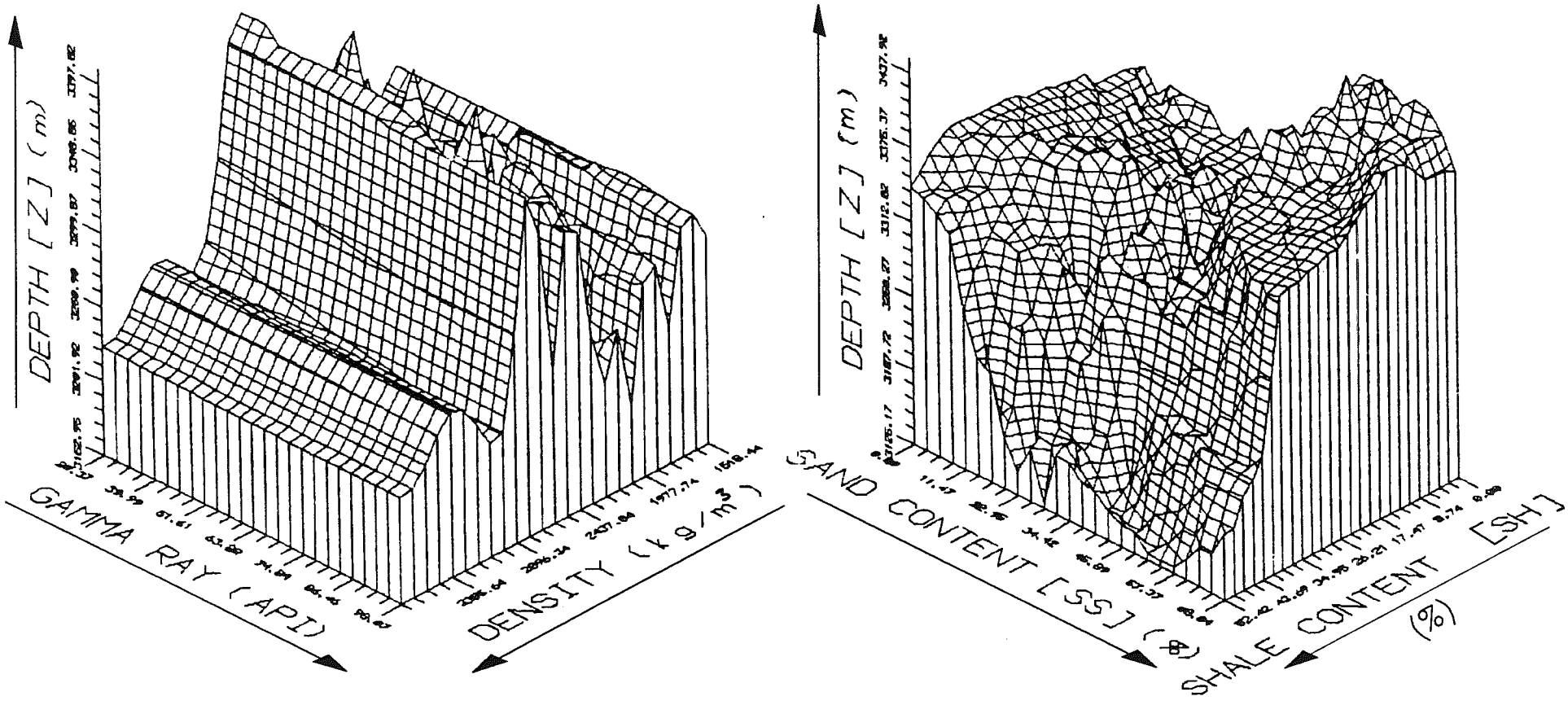

FIGURE (3.1) (cont'd): Bulk density [DEN] - gamma ray [GR] - depth [Z] for well K-07 (E); shale content [SH] - sand content [SS] - depth [Z] for well K-08 (F).

G: TERRA NOVA WELL K-17

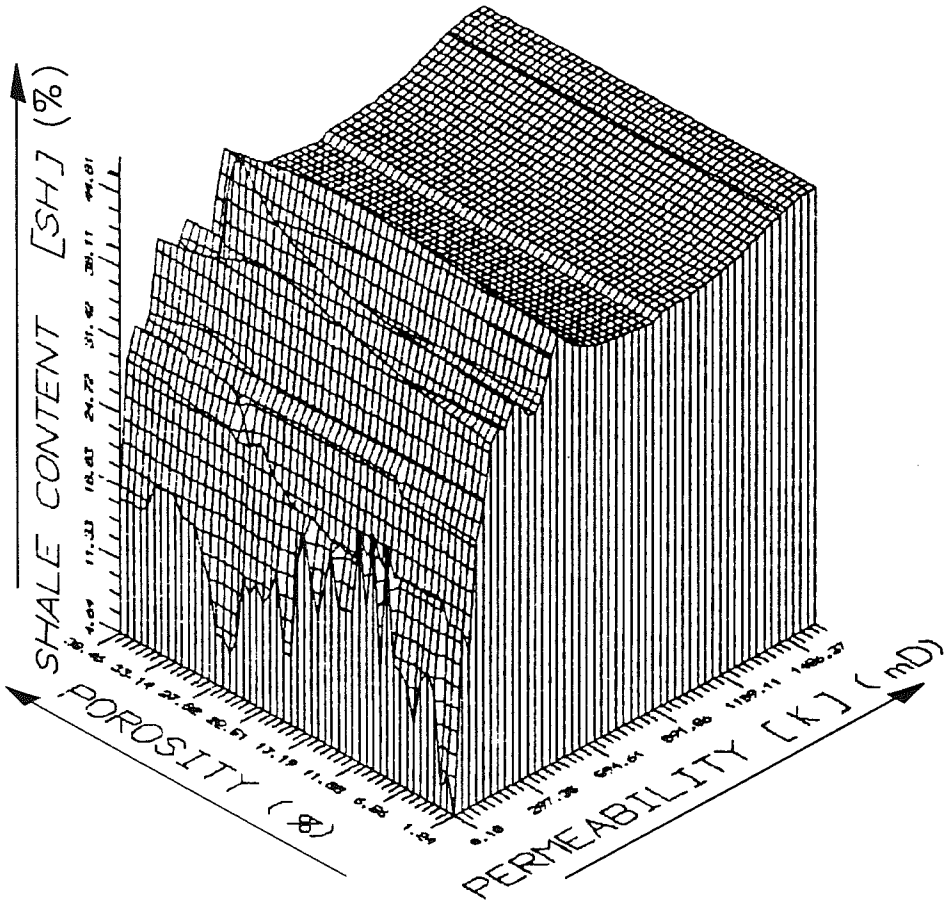

H: TERRA NOVA WELL K-18

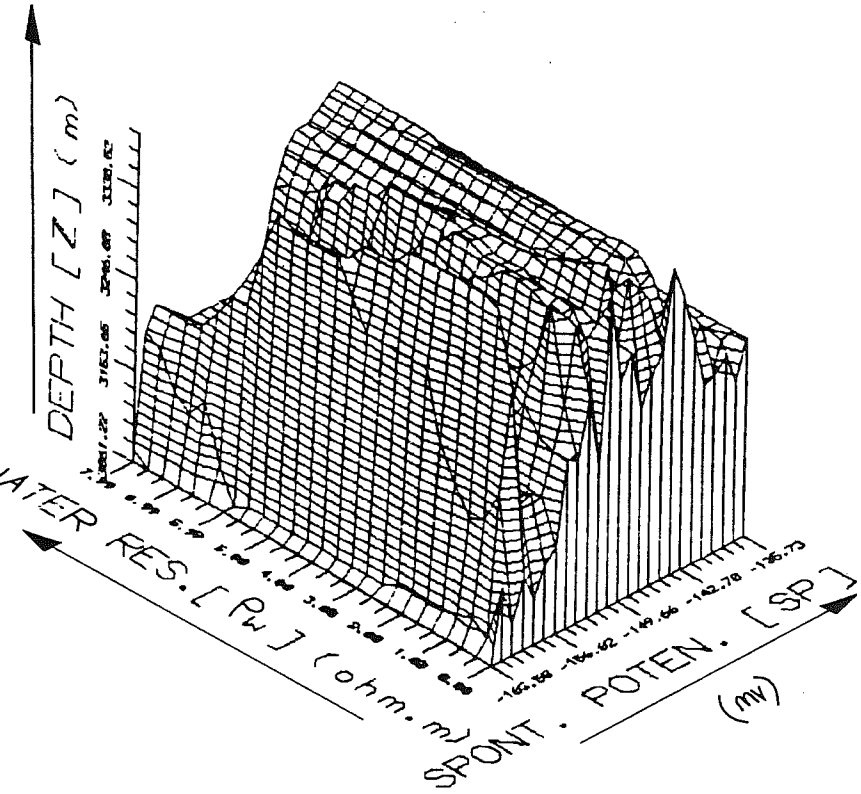

FIGURE (3.1) (cont'd): Permeability [K] - porosity [Φ] - shale content [SH] for well K-17 (G); spontaneous potential [SP] - pore water resistivity [ρ_w] - depth [Z] for well K-18 (H).

A: HIBERNIA WELL B-08

B: HIBERNIA WELL B-27

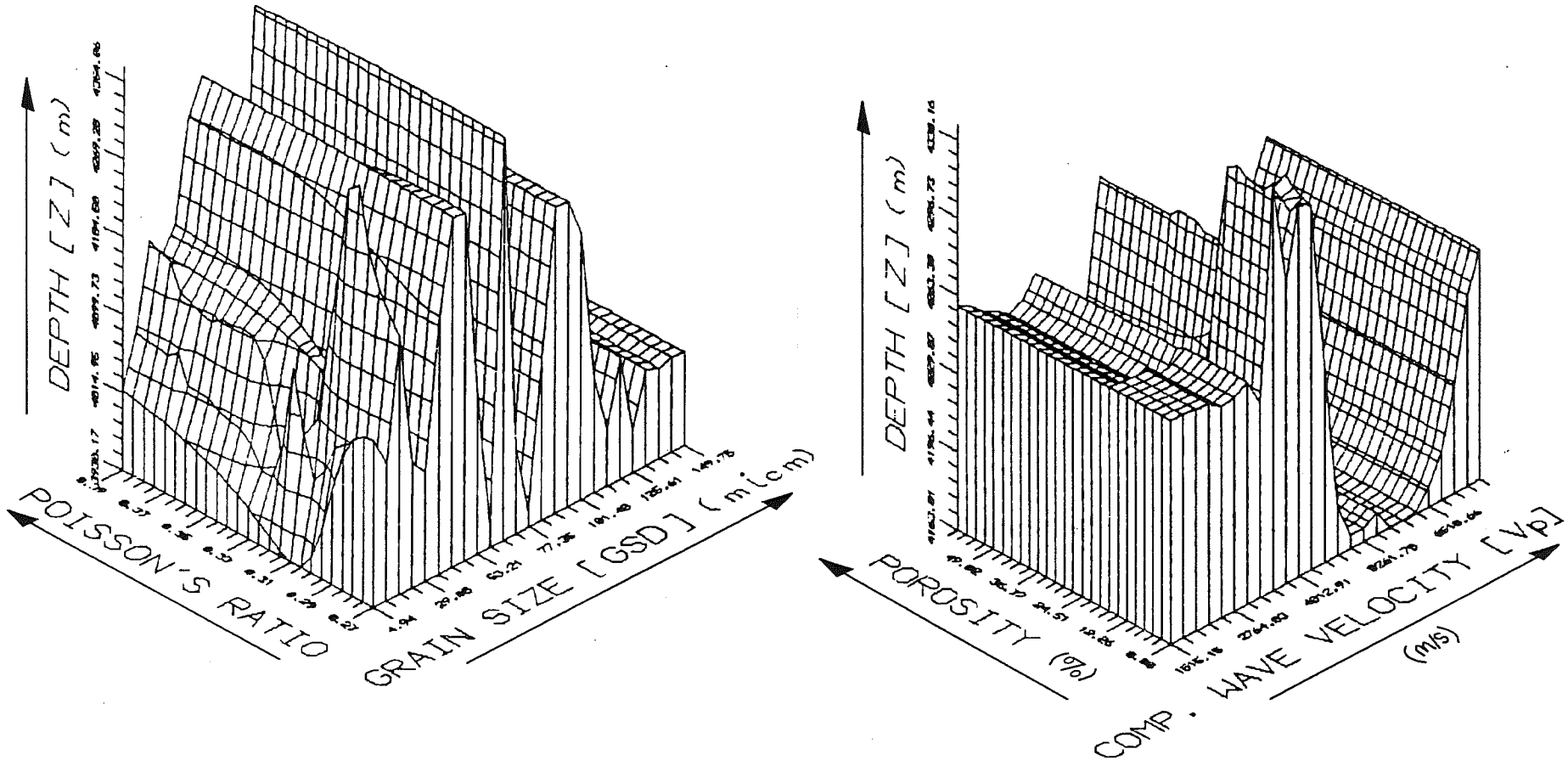

FIGURE (3.2): Three dimensional plots for the Hibernia oil field; mean grain size distribution [GSD] - Poisson's ratio [σ] depth [Z] for well B-08 (A); compressional wave velocity [V_P] - porosity [Φ] - depth [Z] for well B-27 (B).

C: HIBERNIA WELL C-96

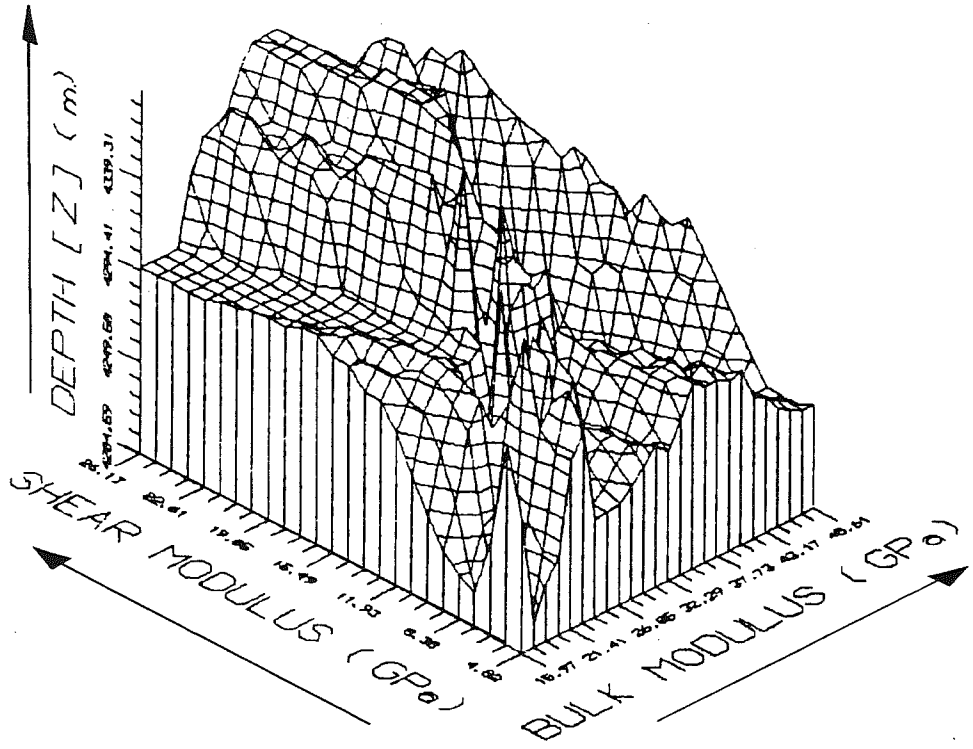

D: HIBERNIA WELL K-14

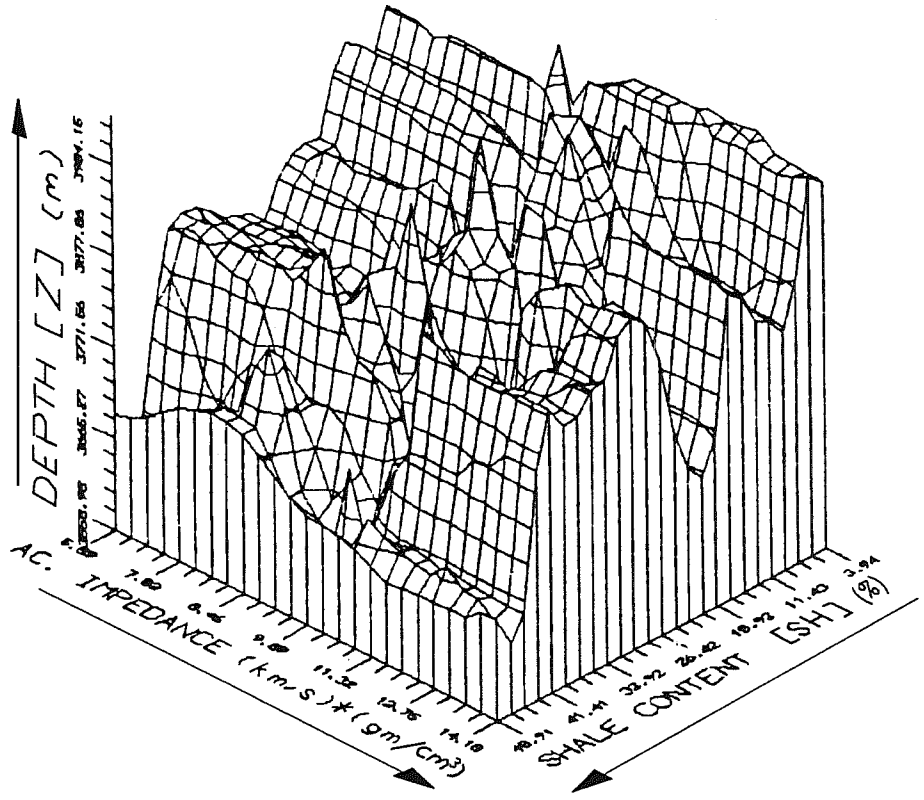

FIGURE (3.2) (cont'd): Bulk modulus [K] - shear modulus [μ] - depth [Z] for well C-96 (C); shale content [SH] - acoustic impedance [Γ] - depth [Z] for well K-14 (D).

E: HIBERNIA WELL K-18

F: HIBERNIA WELL P-15

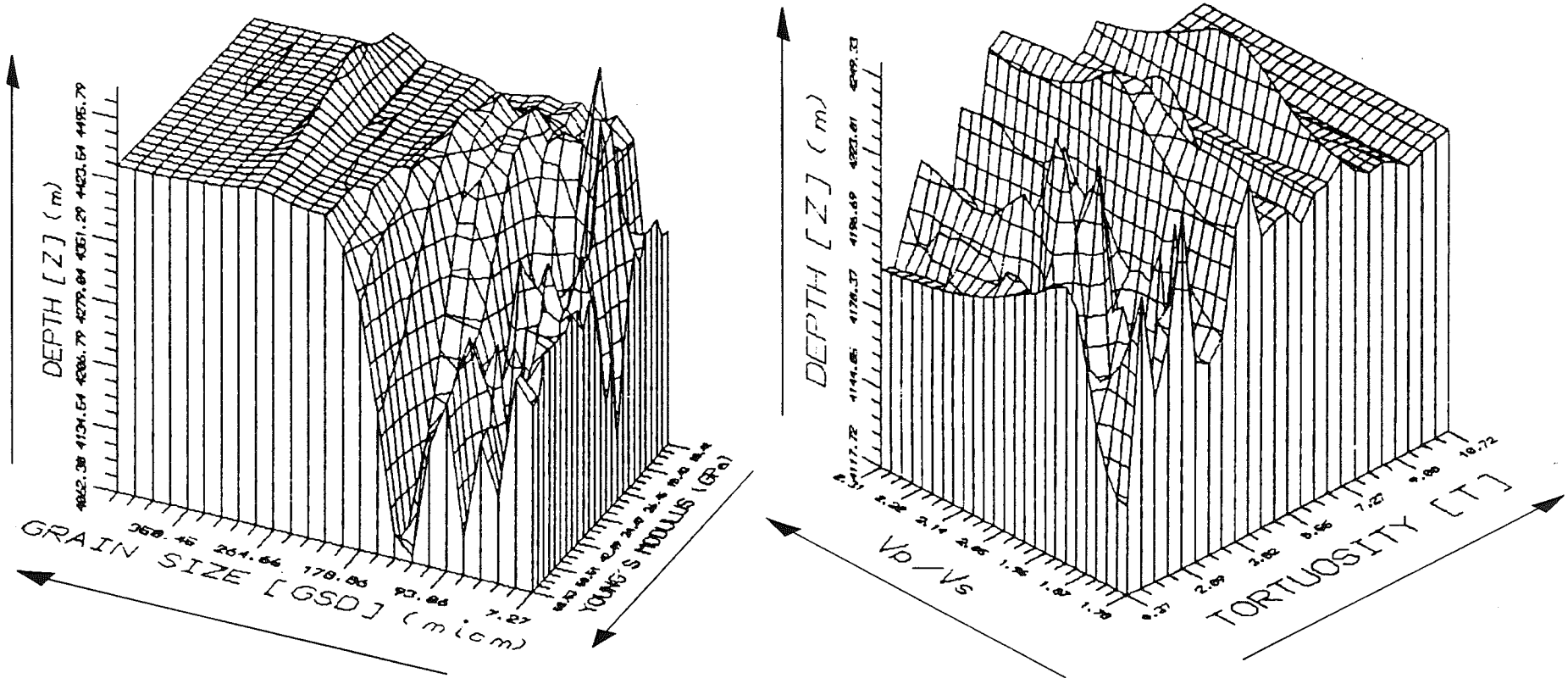

FIGURE (3.2) (cont'd): Young's modulus [E] - mean grain size distribution [GSD] - depth [Z] for well K-18 (E); tortuosity [T] - velocity ratio [V_p/V_s] - depth [Z] for well P-15 (F).